January 2013

Medium Power, Compact Periodic Spiral Antenna

Jonathan O'brien
University of South Florida, jobrien4@mail.usf.edu

Medium Power, Compact Periodic Spiral Antenna

by

Jonathan M. O'Brien

A thesis submitted in partial fulfillment
of the requirements for the degree of
Master of Science in Electrical Engineering
Department of Electrical Engineering
College of Engineering
University of South Florida

Major Professor: Thomas M. Weller, Ph.D.
Gokhan Mumcu, Ph.D.
Huseyin Arslan, Ph.D.
John Grandfield, B.S.E.E.

Date of Approval:
November 8, 2013

Keywords: Three Dimensional Miniaturization, Ultra-Wideband Antennas, Thermal Modeling, Miniaturization Techniques, Loop Antenna

Dedication

To my family

My mother who never let me quit at anything

My father who taught me that life isn't a destination

Joey who made me understand more about life than I could ever explain

My brother for being my best competitor in school

My best sister who can always make me laugh

Acknowledgments

Words cannot express the gratitude and respect I have for my advisor, Prof. Thomas Weller. To say the least, his advice and continuing support throughout this work was the cornerstone to reach my goals. I would like to thank Dr. Gokhan Mumcu for teaching me the fundamentals of antenna theory and always being a knowledgeable source for even the most advanced of questions. I am grateful to my other committee members, Dr. Richard Gitlin and John Grandfield, for reviewing my thesis and participating in my defense.

I am indebted for the financial support that Sciperio, nScrypt, and finally Draper Labs provided during this research. I couldn't ask for a better Draper Labs advisor than John Grandfield. He always provided excellent feedback on my work and inspired me to use abstract thinking in my designs, which this work stemmed from.

Donations from Rogers Corporation provided the substrate materials needed to experiment with design concepts in a cost effective and quick manner.

I would like to thank everyone in the WAMI group who made the transition into graduate school quick and painless. I couldn't ask for a better group of people than David, Maria, Ibrahim, Mike, Eduardo, Evelyn, Abi, Paul, Tim, and Saurabh.

Finally, I would like to thank the people that surround me every day and helped me get to where I am, both intellectually and personally. All of my friends and family that provided that mental break from my work and the one friend that's smart enough to solve any problem, Dan Smith. Last but not least, Kelsey for understanding that I oftentimes work too hard.

Table of Contents

List of Tables

List of Figures

Abstract

Historical, well developed, procedures for RF design have minimal emphasis on exploring the third dimension due to the difficulty of fabrication. Recent material advancements applicable to 3D printing have brought about low-loss thermoplastics with excellent mechanical properties. Research into depositing conductive inks onto arbitrary 3D shapes has achieved resolutions better than 50 μm with conductivity values approaching that of copper cladding. The advancements in additive manufacturing have improved reliability and repeatability of three dimensional designs while decreasing fabrication time. With this design approach other considerations, such as stability and strength, can be concentrated on during the structure design to realize new shapes. The next step in the future of RF research will encompass designing and further understanding the benefits and consequences of using all three dimensions. This could include meandering an antenna element around other electronic components to make the overall package size smaller or integrating an antenna array into a wing.

The design and analysis of the periodic spiral antenna (PSA) takes a look at a specific case of full volume utilization. In this application meandering in the z-dimension allowed the design to become smaller and more efficient than what is achievable with planar methods. This thesis will go into detail on the characterization of the periodic spiral antenna. To exemplify the benefits of meandering in the z-dimension a loop antenna is presented and benchmarked against other miniaturization techniques. Measured results of two different PSA models are presented and remarks on improving fabrication are given. When an antenna is used as a transmitter

incident power will cause thermal generation so a study was conducted to understand how material properties can govern the amount of heat generated.

Chapter 1: Introduction

1.1. Overview

The periodic spiral antenna (PSA) is a design that takes advantage of all three dimensions to allow it to occupy the smallest possible footprint. Based on the growth rate of an Archimedean spiral, the PSA maintains a constant capacitive coupling between adjacent arms while using the z-dimension to introduce additional inductance. This feature allows the PSA antenna to be miniaturized while keeping the input impedance stable throughout the operational band, which is characteristic of spiral antennas. The true miniaturization of the PSA antenna can be seen in the broadside gain. Other miniaturization techniques may shift the lower gain points (-15 dB) down in frequency but have less of an effect on the 0 dB gain frequency. The PSA antenna maintains the same gain curve as a planar Archimedean spiral while shifting it down in frequency.

During the development of the PSA antenna attention was paid to all three dimensions and their effects on the overall wideband performance of the antenna. Since the arms of a planar Archimedean spiral are electrically close capacitive coupling between arms must remain constant to maintain a flat input impedance. Planar meandering of a spiral antenna causes the adjacent arms to vary in distance creating points of reflection along the arms. This can be remedied and the overall capacitive coupling reduced by adopting an exponential growth factor similar to the equiangular spiral antenna. Since the capacitive coupling between arms can be used as a tool for miniaturization this approach will have a larger footprint than the PSA antenna. Due to the capacitive miniaturization advantages of the Archimedean spiral this growth rate was chosen. The z-dimension of the PSA antenna is the tool that increases the inductance along the arms. The

introduction of inductance must also be controlled to minimize localized reflections, which would degrade the return loss. This problem was remedied by using a sinusoidal meandering style that is a function of the angular distance from the center. By making the height in the z-dimension a function of angular distance the center of the antenna becomes planar and has no additional inductance added. This means the wave is gradually slowed down as it travels along each arm which decreases the low frequency operational point of the antenna while leaving the high frequency content intact.

1.2. Thesis Organization

Chapter two begins the discussion of this thesis by introducing some background information on antennas and how they operate. This includes a brief example of resonant antennas and how their current density controls parameters such as radiation pattern and input impedance. The general equation for frequency independent antennas is presented here along with an example of an Archimedean spiral antenna, which is not considered frequency independent but shares many characteristics. This is followed by the discussion of two commonly used miniaturization techniques, dielectric loading and planar meandering. The theoretical limit of miniaturization is explained with Chu's theory which concentrates of relating spherical volume to quality factor.

Chapter three contains the discussion on thermal effects of RF power on a microstrip. This study includes a parametric analysis of material properties and relates thermal generation to well known RF equations. The information in this section can be used as a guideline to reduce heat generation on a microstrip. Though this study concentrates on a matched 50 Ω microstrip line many of the concepts can be translated to antenna design.

Chapter four presents an equivalent circuit model for the periodic spiral antenna which is used for a parametric study to quantify how inductance and capacitance are changed with the antenna coefficients. To exemplify the benefits of meandering in the z-dimension a square loop antenna was developed since a spiral antenna can be thought of as a series of concentric loops. The meandered square loop antenna was benchmarked against other miniaturization methods and used to see the limits of miniaturization in that particular design. Once the effectiveness of meandering in the third dimension is established the periodic spiral antenna is presented. This includes a study into the effect of changing the amplitude growth profile and its role into the wideband performance of the spiral. A modified cavity design is also presented that allows for improved performance while making the radiation unidirectional. Measurements of a linear and non-linear growth profile PSA antenna show promising results.

1.3. Contribution

The main contribution of this work is the development using the third dimension to miniaturize an antenna. This design technique is proven in both a resonant and ultra-wideband structure with the simulation of a square loop antenna and the fabricated periodic spiral antenna. The periodic spiral antenna has shown to have improved antenna parameters as well as a smaller footprint than other planar miniaturization techniques.

Chapter 2: Background Review

2.1. Introduction

An antenna is the point in an RF system that connects the guided transmission of waves along a conductor with the unguided transmission of waves in free space. This means an antenna should be able to transmit and receive radio waves without discrepancy or introducing undesired effects. In this chapter some fundamental principles of antenna design are presented. A brief coverage of current density and its relationship to radiation is presented with more information found in [1]. This is followed by an explanation of two of the most common forms of miniaturization techniques accompanied by examples. The chapter concludes on the presentation of the theoretical limits of miniaturization presented by Chu. Since all antennas are bi-directional, in terms of transmitting and receiving signals, this work will use terminology for the transmitting mode [1].

2.2. Antenna Operational Principles

Antennas can be separated into different categories based on their theory of operation. Categories such as resonant and frequency independent antennas have been studied and are well understood. Both of these categories have a unique set of advantages and disadvantages in the architecture of a RF system. For example, resonant antennas are narrowband which means they can be selective of the frequency content that is available at the receiver. This can allow the receiver to be simplified by eliminating some of the hardware required for wideband systems, like image frequency suppression prior to the down conversion stage [2]. Frequency independent antennas are inherently broadband and in theory scalable to any range of frequencies. This can

allow the receiver to handle the selection of required frequencies giving way for the system to be more robust in its capabilities [3].

Resonant antenna structures operate by establishing a portion of the wave along the conductor. For example, the dipole and patch antenna resonate when half of the guided wavelength is established along the aperture while the loop antenna will resonate when the structure is one wavelength in circumference [1]. Figure 2.1 shows the current distribution along these antenna structures. Due to this characteristic the antennas become narrowband since deviation from the center frequency causes a change in the guided wavelength. The current density of the antenna can also influence where the feed point of the antenna should be located. Examining the current distribution of the patch antenna in Figure 2.1 a current minimum is observed at the edges of the patch. Due to Ohm's Law this is then the location for a voltage maximum, corresponding to a high impedance value [1]. The center of the patch exhibits exactly the opposite in terms of voltage and current and is the location for a zero impedance value. Further understanding of the sinusoidal current density between these two points shows that there will be a location that exhibits 50Ω simplifying the feed network required.

To generate radiation from an antenna constructive interference must be made in the far-field. In the far field of these antennas the current distribution causes the radiation pattern to be normal to the aperture i.e. peak radiation in the broadside. To understand the radiation pattern of a half wavelength dipole antenna along the z-axis the electric and magnetic far-field components are shown in equations (2.1) and (2.2), respectfully [1]. This equation shows that the radiation pattern is independent of ϕ and has a maximum at $\theta = \pi/2$ creating a donut shaped radiation pattern normal to the aperture of the antenna.

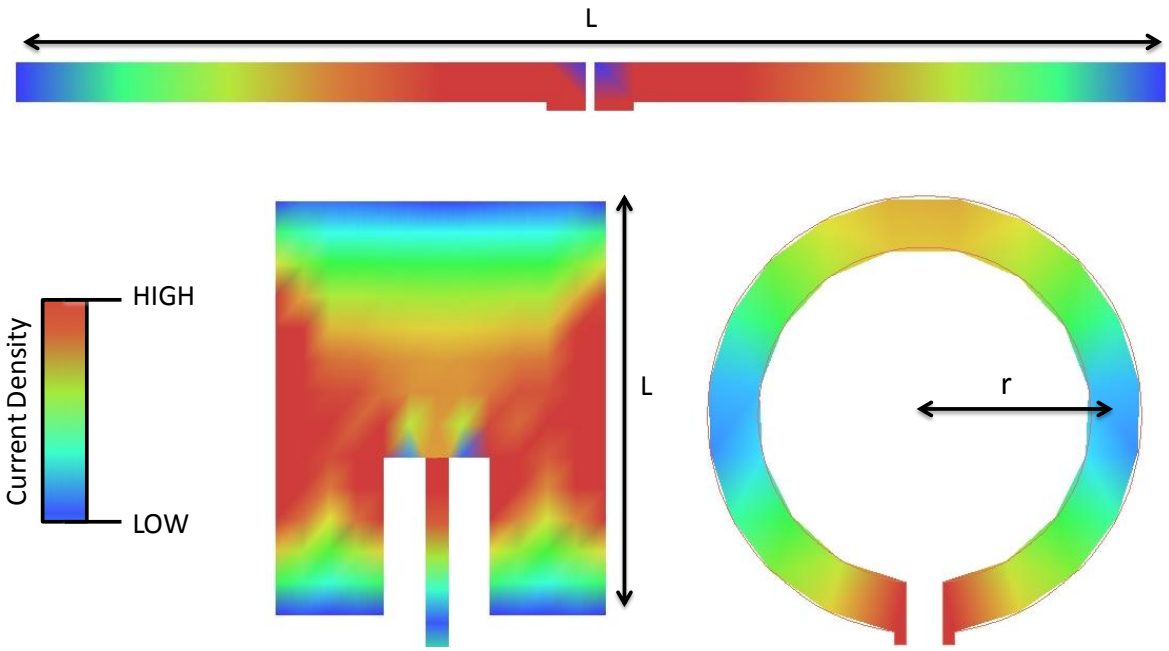

Figure 2.1: Current distribution of dipole (top), patch (bottom left), and loop antenna (bottom right)

$$E_\theta \cong j\eta \frac{I_0 e^{-jkr}}{2\pi r}\left[\frac{\cos\left(\frac{\pi}{2}\cos\theta\right)}{\sin\theta}\right] \tag{2.1}$$

$$H_\phi \cong j\frac{I_0 e^{-jkr}}{2\pi r}\left[\frac{\cos\left(\frac{\pi}{2}\cos\theta\right)}{\sin\theta}\right] \tag{2.2}$$

Frequency independent antennas are a classification of antennas that are specified by angles and exhibit a very large bandwidth [1]. In theory these antennas can be scaled to any frequency range by an inverse scaling of physical size. To be more specific a frequency independent antenna must be described by equation (2.3), according to [1], where r is the radius from the origin of the antenna. Certain frequency independent antennas, such as the planar equiangular antenna, are popular due to their wideband characteristics like polarization, gain, return loss, and constant radiation pattern. Many ultra-wideband antennas, like the Archimedean spiral antenna shown in Figure 2.2, exhibit wideband antenna parameters but are not considered

frequency independent since they do not follow the fundamental equation set in (2.3). More information on frequency independent antennas can be found in [1].

$$r = F(\theta, \phi) = e^{a\phi} f(\theta) \tag{2.3}$$

$$\text{where } a = \frac{1}{K}\frac{dK}{dC}$$

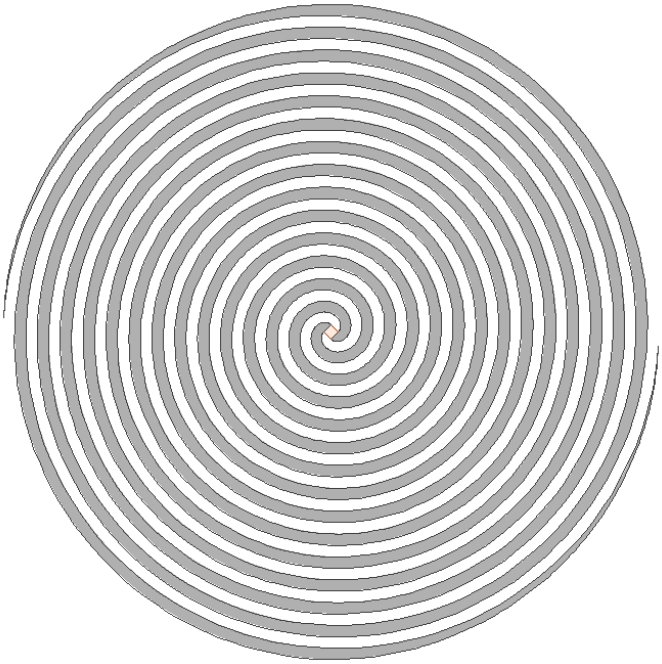

Figure 2.2: Layout of Archimedean spiral antenna

2.3. Antenna Miniaturization Techniques

There are many different, well understood, techniques for miniaturizing an antenna. Some of the most common methods include dielectric loading and meandering of the element [4] [5]. It is also well known that miniaturization of an antenna comes at the cost of reduced bandwidth, efficiency, gain, etc [6]. This section will help to build a conceptual understanding of these two

commonly employed miniaturization techniques and show examples of how each technique is used.

Dielectric loading is commonly the first form of miniaturization applied to an antenna design, shown in Figure 2.3. The electrical length, βl, along a guided transmission line is proportional to $\sqrt{\varepsilon_{eff}}$, see equation (2.4) [7]. This shows that as the effective permittivity increases along a fixed length transmission line the electrical length will also increase. In terms of the $\lambda/2$ dipole antenna the physical length of the antenna can be reduced to maintain half of a wavelength along the conductor. Three ways to increase the effective permittivity of the antenna are to increase the substrate height (d), increase the relative permittivity of the substrate (ε_r), or use a substrate as well as a superstrate [8]. When referring to a lumped element transmission line model, seen in Figure 2.4, this is explained as an increase in capacitance per unit length and the wave velocity is calculated by equation (2.5). A parallel plate capacitor can be referenced here to explain how dielectric loading is related to capacitance. A parallel plate capacitor is defined as two different potential conductors separated by a distance, d, which is filled with a material of relative permittivity ε_r [7]. The amount of capacitance present in a parallel plate capacitor is shown in equation (2.6) which shows that as the effective permittivity is increased the capacitance is increased.

$$\beta l = k_0 \, l \sqrt{\varepsilon_{eff}} \tag{2.4}$$

$$v_p = \frac{1}{\sqrt{L\,C}} \tag{2.5}$$

$$c = \frac{w\,\varepsilon}{d} \tag{2.6}$$

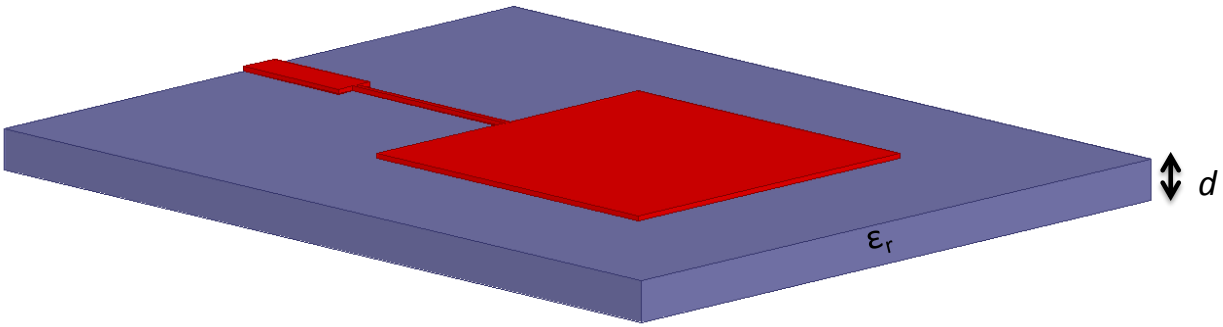

Figure 2.3. Example of a patch antenna loaded with a dielectric substrate of permittivity, ε_r, and thickness, *d*.

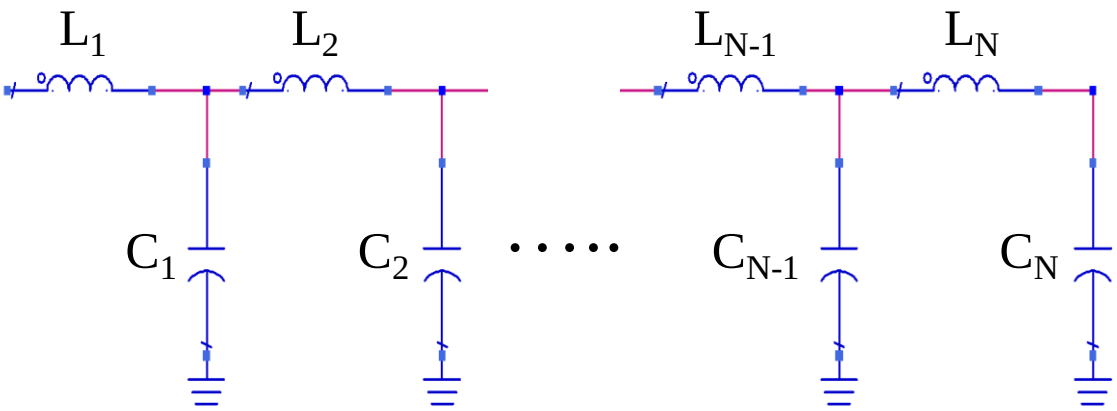

Figure 2.4: Equivalent circuit model of lossless transmission line

Meandering of the antenna element is another popular form of miniaturization. This technique involves arranging the element in a style that decreases the dimensions of the antenna by meandering the length of the conductor. An example of a meandered loop antenna can be seen in Figure 2.5. Another example of a meandered antenna can be seen in [4]. This style of miniaturization is referred to as inductive loading in a lumped element transmission line model due to the increase in inductive transmission line along a fixed length. The benefit of relating miniaturization techniques to a lumped element model has been exploited by using artificial transmission lines. Artificial transmission lines are created by the use of a series inductor and

shunt capacitor in a unit cell that is then cascaded [9]. This technique allows the designer to control both the velocity of propagation and impedance of the transmission line. An application of this technique in an antenna structure can be seen in [9].

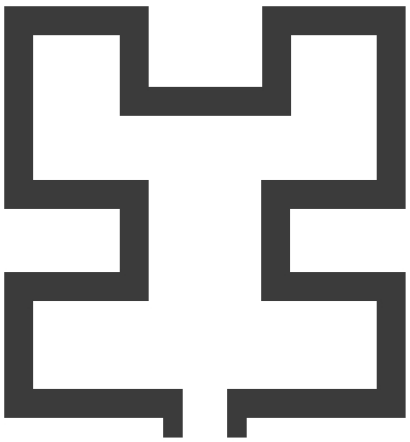

Figure 2.5: Layout of planar meandered loop antenna

2.4. Miniaturization Limits

When miniaturizing an antenna design both inductive and capacitive loading are needed to achieve the maximum level of miniaturization where the limit of miniaturization has been studied and defined with Chu's theory and Wheeler's theory [10] [11]. Wheeler's work on the limit of antenna miniaturization was done first and concentrated on very small antennas. This theory used either a capacitor or an inductor along with a resistor to model the antenna [10]. Chu's theoretical limit then expanded to use the quality factor of the antenna to explain the relationship between electrical size and effectiveness as a radiator [11].

The quality factor of any RF device is a measure of how much energy is lost per unit time. For antenna applications a low quality factor means that the structure is radiating energy effectively. To estimate the quality factor of an antenna by its physical size a sphere is used to

encompass the largest part of the antenna where *a* is the radius, shown in Figure 2.6. Equation (2.7) then estimates the quality factor of the antenna using the radius of the encapsulating sphere [1]. For electrically small antennas, defined as *ka* << 1, this equation is simplified. Chu's limit shows that as *ka* is decreased the quality factor of the antenna is increased making it less effective as a radiator. Figure 2.7 shows a graph of the quality factor of an antenna as the electrical size is decreased [1]. This information leads to the important realization that in order to increase the overall efficiency of a miniaturized antenna all three dimensions must be properly utilized. More information on an antennas quality factor can be found in [12] [13].

$$Q = \frac{1+2\,(ka)^2}{(ka)^3\,[1+\,(ka)^2]} \;\; for\; ka \ll 1 \; Q = \frac{1}{(ka)^3} \tag{2.7}$$

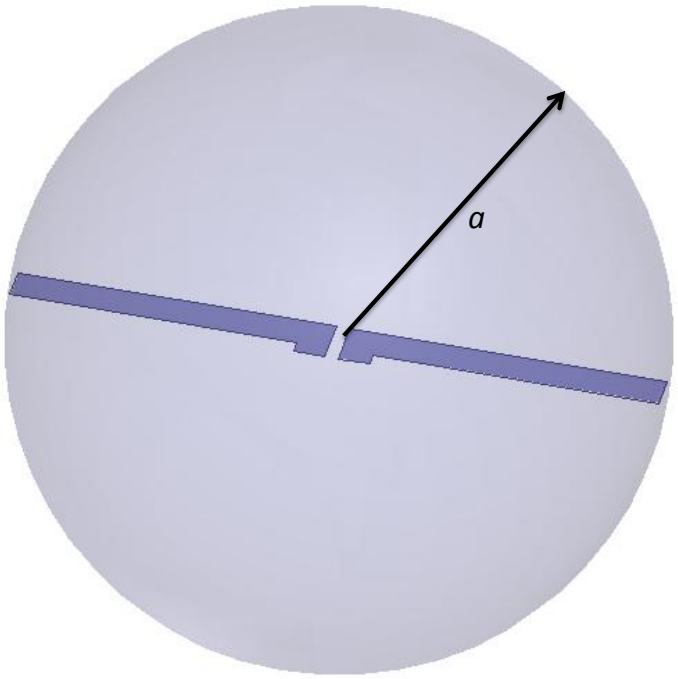

Figure 2.6: Sphere containing the antenna where *a* is the radius of the sphere

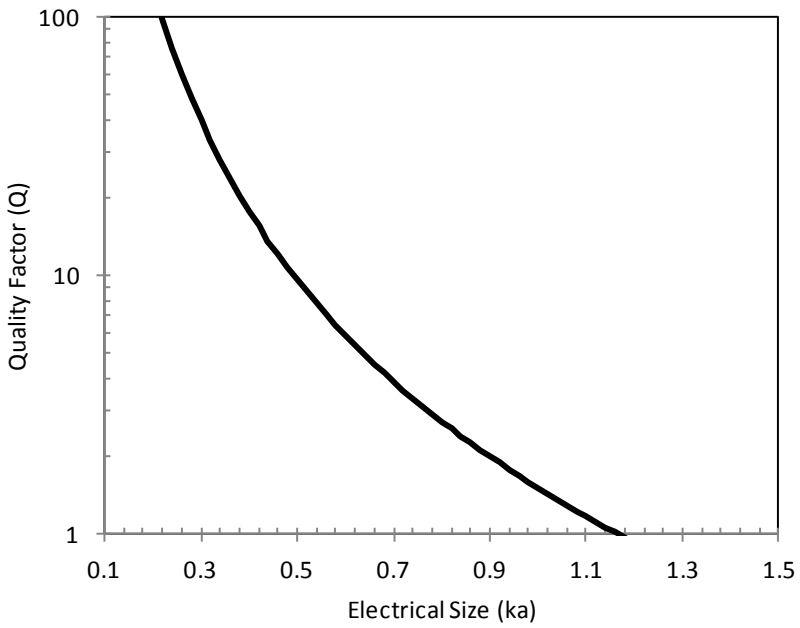

Figure 2.7: Theoretical quality factor limit versus antenna size. Derived from [1].

2.5. Conclusion

The design and miniaturization of antennas requires an understanding of the electromagnetic fields on the antenna structure. A $\lambda/2$ dipole antenna has a current maximum at the feed point of the antenna and decays to a minimum at the ends. This behavior controls parameters such as input impedance, radiation pattern, and directivity. To miniaturize the design this chapter explored two common planar techniques, capacitive and inductive loading, which come with a tradeoff in decreased antenna performance. Due to the relationship between quality factor and sphere size (*ka*) defined by Chu higher efficiency miniaturization can be achieved by using all three dimensions during the design process.

Chapter 3: Thermal Modeling

3.1. Introduction

The effects of RF power on the performance of the microwave structure can include voltage breakdown, fluctuations in relative permittivity, and phase transition of the substrate. Proper thermal modeling of the antenna structure can help the designer to understand the cause of heat generation and employ techniques to reduce the amount of heat in the structure. In this chapter Ansys Workbench 14.5 will be used to simulate the steady state thermal values of a structure and a parametric analysis into the effect of different material properties will be done.

3.2. Thermal Design Considerations

One of the contributing factors for the amount of heat present in a microstrip structure is the thermal conductivity of the substrate. Thermal conductivity (k) is a material property that governs the rate of heat transfer inside the volume of a material [14]. The amount of heat transferred within a material is governed by the law of thermal conduction and defined by equation (3.1) where A is the cross sectional area, $|dT/dx|$ is the temperature gradient, and $\mathcal{P}$ has units of watts. It can be seen from this equation that the thermal conductivity provides a scalar constant for the amount of heat that can be transferred away from the heat source and into the surrounding body. Once thermal energy reaches the boundary between the material and the surrounding environment Newton's Law of Cooling provides a quantitative explanation of the rate of transfer across this boundary [14]. Equation (3.2) shows Newton's Law of Cooling where h_c is the convective heat transfer coefficient and dT is the temperature difference between the surface of the material and the surrounding environment.

$$\mathcal{P} = kA \left|\frac{dT}{dx}\right| \tag{3.1}$$

$$q = h_c \, A \, dT \tag{3.2}$$

Conservation of energy states that the change in the total energy of the system is equal to the amount of energy that is transferred across the system boundary into another system [14]. More specifically, inside the system energy cannot be created nor destroyed only be transformed into another type of energy, e.g. electrical energy dissipated is transformed into thermal energy. In a microstrip line it will be shown that the attenuation present along a microstrip line is related to the heat generated in the structure.

Transverse electromagnetic (TEM) propagation along a microstrip line is explained with equations (3.3) through (3.6) [7]. Using these equations the power loss along a transmission line can be described by equation (3.7) where Γ is the reflection coefficient [7]. In a lossy structure the complex propagation constant γ consists of two components, the attenuation constant and the phase constant. The real part, α, is the attenuation constant of the wave and can be decomposed into three individual loss factors; conductor loss (α_c), dielectric loss (α_d), and radiation loss (α_r) [7]. See equation (3.5) and equation (3.6). In most microstrip designs radiation loss is minimal and can be ignored. When designing antenna structures radiation loss is significant and must be accounted into the attenuation of the wave along the transmission line but does not contribute to the amount of heat generated. The remaining two loss factors are the source of heat generation in a microstrip structure and will be further investigated. More information regarding losses in a microstrip can be found in [15] [16].

$$V(z) = V_o^+ e^{-\gamma z} + V_o^- e^{\gamma z} \tag{3.3}$$

$$I(z) = I_o^+ e^{-\gamma z} + I_o^- e^{\gamma z} \tag{3.4}$$

$$\gamma = \alpha_t + j\beta \tag{3.5}$$

$$\alpha_t = \alpha_c + \alpha_d + \alpha_r \tag{3.6}$$

$$P_{loss} = P_{in} - P_L = \frac{|V_o^+|^2}{2Z_o}[(e^{2\alpha l} - 1) + |\Gamma|^2(1 - e^{-2\alpha l})] \tag{3.7}$$

Attenuation due to conductor loss will have a direct impact on heat generation in the structure. The amount of heat generated on the conductor is correlated to equation (3.8) where *Rs* is sheet resistance [7]. This equation shows that to reduce conductor loss, and therefore the amount of a heat generated, a wider microstrip line can be used. This assumes the conductor thickness is greater than a few skin depths. Equation (3.10) shows that to maintain a fixed impedance while increasing the width of the microstrip line a thicker substrate or one with a low dielectric constant must be used. Oftentimes when designing compact microwave structures a low dielectric constant is not beneficial so a tradeoff between physical size and heat generation must be made. Another way to reduce the amount of heat generated on a transmission line with a fixed set of dimensions is the increase the conductivity. This can be accomplished by choosing another conductive material or plating the metal with a highly conductive coating, such as gold.

$$\alpha_c = \frac{R_s}{Z_o W} \; Np/m \tag{3.8}$$

$$\text{where } R_s = \sqrt{\omega \mu_o / 2\sigma}$$

Attenuation due to dielectric loss will also have a direct impact on heat generation in the structure. Equation (3.9) describes the losses from the dielectric medium for a quasi-TEM wave

where F is a "filling factor" that accounts for the part of the fields that are present in the lossless air [7]. From here it can be seen that the loss tangent, tanδ, of the substrate has a linear effect on the amount of loss in the substrate and therefore amount of heat generated. The use of high quality, low loss microwave substrates can significantly reduce this contribution without any compromise in physical size.

$$\alpha_d = \frac{k_o \epsilon_r (\epsilon_e - 1) tan\delta}{2\sqrt{\epsilon_e}(\epsilon_r - 1)} = F * \frac{k_o tan\delta}{2} \; Np/m \tag{3.9}$$

where k_o is the wave number.

According to the presented equations to reduce the heat generated along the transmission line a wider microstrip line with a higher conductivity can be used. In order to do this a lower dielectric constant must be chosen to maintain the impedance. To reduce the heat generated inside the substrate a low loss microwave substrate can be used.

3.3. Thermal Modeling Methods

Proper modeling of the thermal effects due to attenuation inside a microwave structure can provide an understanding of the heat source and provide a basis for improvement. General guidelines for controlling the amount of heat that is generated in a microwave structure were covered in section 3.2. In the next section Ansys Workbench 14.5 is used to simulate steady state temperatures in a microwave structure. Ansys Workbench 14.5 is a numerical tool that utilizes the loss data created during a full wave HFSS simulation. This data is used to calculate the amount of heat generated in the structure and uses the convection boundary condition specified by the user to reach a steady state temperature. More information on how to set up a steady state thermal simulation using Ansys Workbench 14.5 can be found in [17]. This data can then be fed

back into HFSS and used to implement any thermal drift that occurs in the material properties to get a more accurate simulation of the RF performance.

3.4. Thermal Trends in Microwave Structures

To begin to understand the heat generation associated with RF power dissipation a parametric study has been performed. For this study a substrate was designed to have a width, W,of 25.4 mm (1 in) and a length, L, of 50.8 mm (2 in) so that it had a sufficient width and length to observe a temperature gradient. As a wave is propagating along a lossy transmission line it is expected to decay as a function of position. Due to this reason temperature is also expected to decay as a function of position leading to the conclusion that the highest temperature will be present at the point of insertion. This can be seen in Figure 3. The material properties and height of this substrate were then varied while maintaining a characteristic impedance of 50Ω with a return loss better than 20 dB across the frequency range to reduce heat generation due to reflections. An in depth study on the thermal effects of characteristic impedance on a transmission line is shown in [18]. To ensure proper isolation of the material property being studied all other material properties were set to the values specified in Table 3.1.

This study was done as an introduction to understand relationships between material properties and their effects of thermal generation. It is important to understand the electrical and thermal limitations of the individual materials being used to be able to design a structure that can withstand high power. Other phenomenon such as large reflection due to discontinuities can cause excess heat to be generated at along the transmission line as well as increased voltages which can lead to dielectric breakdown of the substrate.

Table 3.1: Control variables for the microstrip thermal study

Relative Permittivity	5
Loss Tangent	0.02
Conductivity (S/m)	5.80E+07
Thermal Conductivity	0.25
Thickness (mils)	60
Power (W)	30

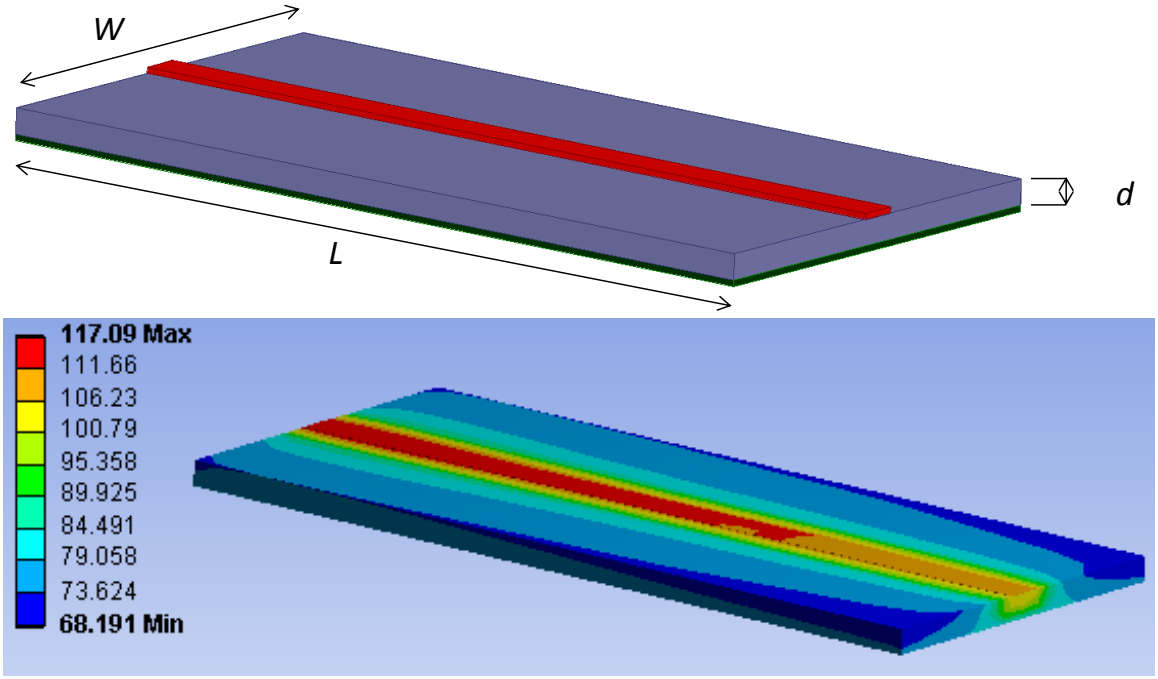

Figure 3.1: (Top) Layout of test substrate and (Bottom) Thermal gradient when 30 watts of power at 3 GHz is incident on the left side of this figure

3.4.1 Relative Permittivity

The permittivity of the substrate plays a major role in the width required for a controlled impedance transmission line. This relationship is explained with equation (3.10). It can be seen here that the width of the microstrip line in inversely related to the effective dielectric constant (ϵ_e). According to equation (3.8) a higher effective permittivity would mean a higher conductor attenuation coefficient (α_c) resulting in higher temperatures on the structure. Here the relative permittivity of the substrate was swept from 2 – 10 while keeping all other material properties

and dimensions the same. Simulation results are shown in Figure 3.2. This data shows that the temperature varies from 74 °C to 159 °C at 3 GHz when increasing the relative permittivity from 2 – 10. This range of permittivity corresponds to a conductor width ranging from 198 mils to 60 mils.

$$Z_o = \frac{60}{\sqrt{\epsilon_e}} \ln\left(\frac{8d}{W} + \frac{W}{4d}\right) \qquad for\ W/d \leq 1 \tag{3.10}$$

$$\text{where } \epsilon_e = \frac{\epsilon_r + 1}{2} + \frac{\epsilon_r - 1}{2} \frac{1}{\sqrt{1+12d/W}}$$

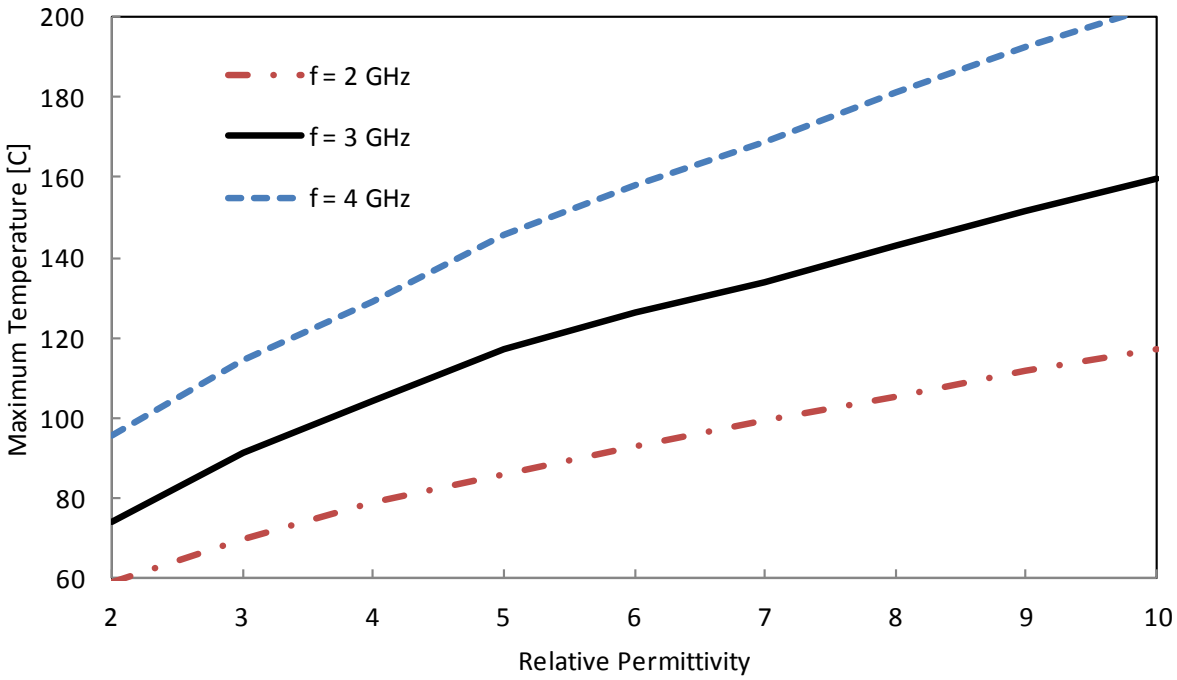

Figure 3.2: Maximum temperature in the microstrip structure as a function of relative permittivity of the substrate

3.4.2 Conductivity

Referring to equation (3.8) the conductivity of the material has an inverse exponential relationship to the conductor attenuation constant. To understand the thermal effects of

conductivity a range was specified to range from a value much less than copper (4.5E5 S/m) to a value much higher than readily available conductors. Results are shown in Figure 3.3 and a small change in temperature is observed compared to the other material properties studied. Specifically, a change in conductivity from 4.5E6 S/m to 4.5E8 S/m corresponds to a decrease in temperature from 131 °C to 113 °C at 3 GHz, respectfully. This trend can be verified when apply equation (3.8).

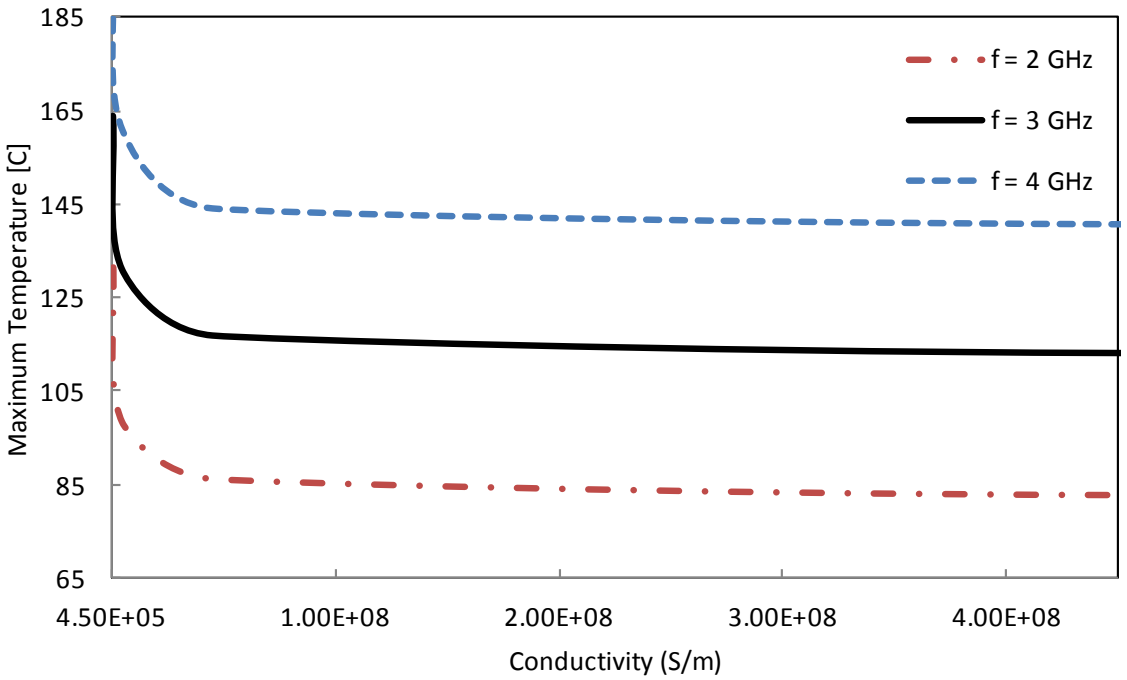

Figure 3.3: Maximum temperature in the microwave structure as a function of conductivity

3.4.3 Loss Tangent

The loss tangent of a substrate determines the amount of attenuation present in the dielectric. Since it was shown in Figure 3.3 that conductivity has a minor role in heat generation the loss tangent of the material is expected to be the major contributor. According to equation (3.9) the attenuation due to the dielectric should have a linear correlation to the loss tangent of

the material. Results of this parametric study are shown in Figure 3.4. The trend of this data agrees with equation (3.9) and shows that as the loss tangent is increased the heat generated is also increased. For example, this data shows that an increase in loss tangent of 0.005 results in a temperature increase of 22.3 °C at 3 GHz. A typical low-loss microwave laminate has a loss tangent below 0.005 while FR-4 is above 0.02 resulting in a temperature difference of 67.2 °C.

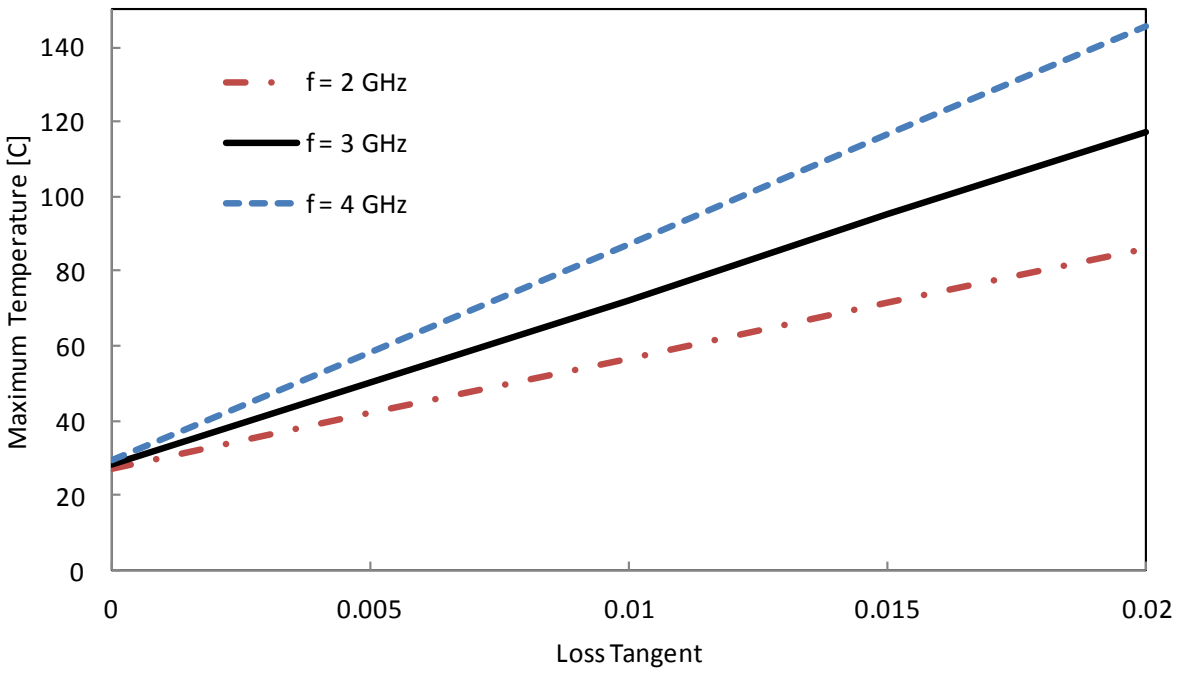

Figure 3.4: Maximum temperature in the microwave structure as a function of substrate loss tangent

3.4.4 Substrate Thickness

As the thickness, d, of the substrate is increased the width of the conductor must also increase to maintain a specified impedance. This is synonymous to a decrease in dielectric constant. The thermal effect of increasing the conductor width with a fixed substrate thickness has already been studied and shows a decrease in temperature; these results were displayed in Figure 3.2. This study will quantify the interaction between the conductor and dielectric

attenuation constants as substrate thickness is increased. Figure 3.5 shows that increasing the thickness of the substrate will result in a small decrease in temperature. For completeness this figure shows multiple values of dielectric loss tangent to ensure this trend is accurate for both low loss and medium loss substrates.

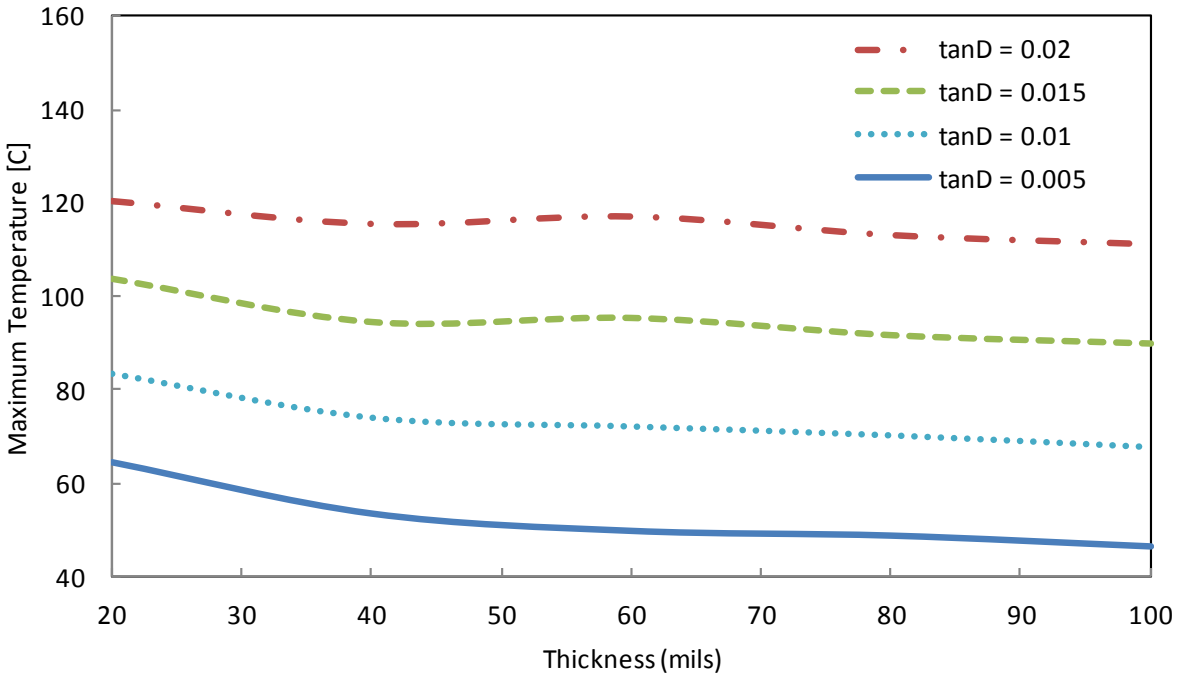

Figure 3.5: Maximum temperature in the microwave structure as a function of substrate thickness

3.4.5 Thermal Conductivity

The thermal conductivity (k) is a material property that governs the rate of heat transfer within a material. A table listing thermal conductivity values of commonly used dielectric and conductor materials can be found in [19]. The effects of varying the thermal conductivity in the test substrate can be seen in Figure 3.6. Referring back to equations (3.1) and (3.2) the amount of heat that is dissipated from a structure is a function of both the internal thermal conductivity of the material as well as the convective heat transfer coefficient of the surrounding environment.

Therefore increasing the thermal conductivity of the material will result in a diminishing return since the limiting factor becomes the convective heat transfer coefficient of the environment.

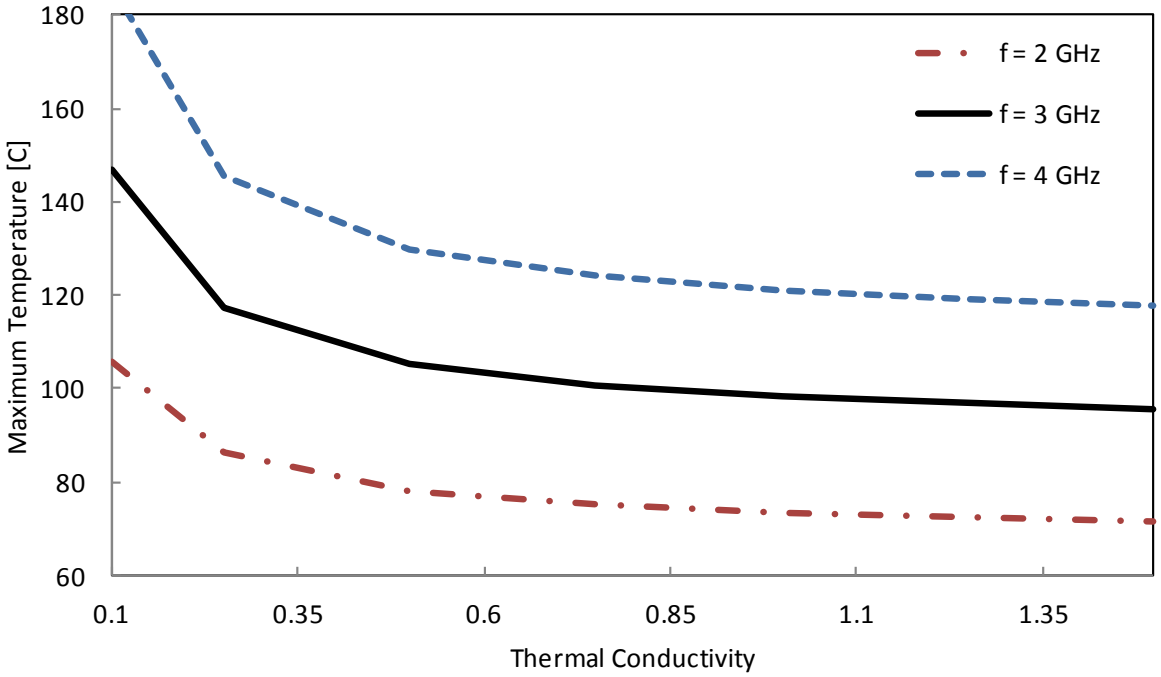

Figure 3.6: Maximum temperature in the microwave structure as a function of thermal conductivity

3.4.6 Frequency Response

The frequency components in both the dielectric and conductor attenuation constants show an increase in loss as a function of frequency. To see how frequency affects heat generation a frequency sweep was done and different dielectric constants were studied. Results can be seen in Figure 3.7. This data supports equations (3.8) and (3.9) showing the expected correlation between frequency and temperature.

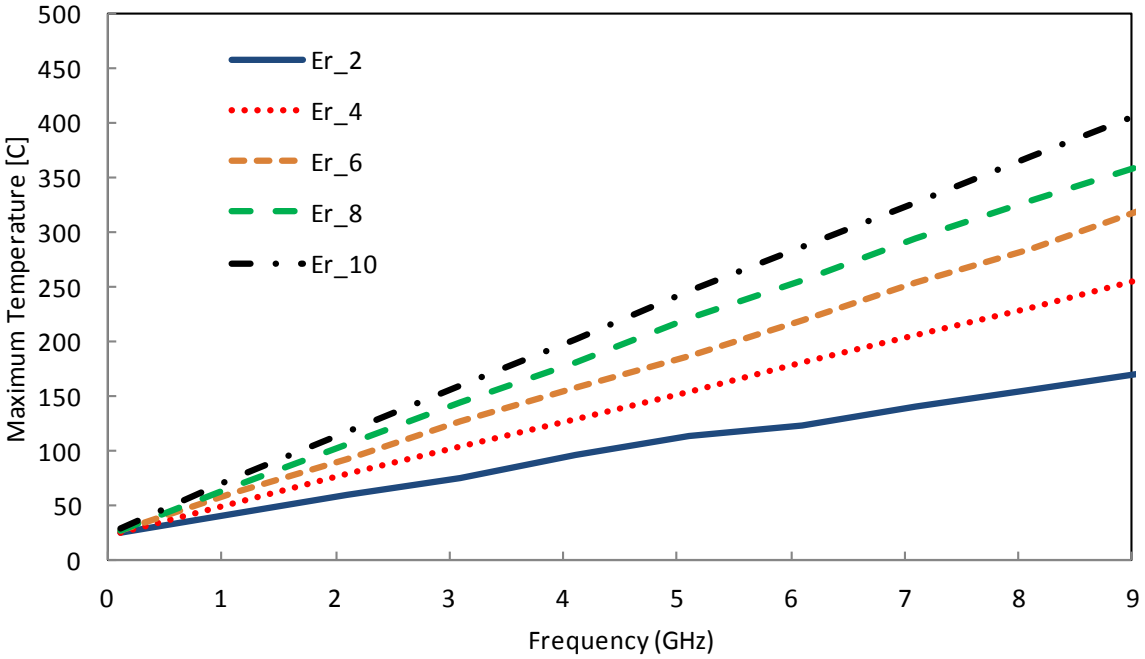

Figure 3.7: Maximum temperature in the microwave structure as a function of frequency with different dielectric constants

3.5. Conclusion

The data presented here creates some guidelines for high power microstrip design. The most important factor is to reduce the amount of heat generated by using a low loss substrate with the lowest relative permittivity allowable by the design specifications. This will allow the conductor to be wider so the conductor and dielectric attenuation will be minimized. Further improvements can then be made by using a substrate that has an increased thermal conductivity to allow the heat to be transferred away from the source more efficiently.

Chapter 4: Periodic Spiral Antenna Design

4.1. Introduction

Traditional techniques to antenna miniaturization, which include planar meandering and dielectric loading, were covered in chapter 2. In this chapter some examples of utilizing the third dimension to miniaturize an antenna are covered. This technique oftentimes results in an overall smaller package size and allows the antenna design to conform around other system level electronics. An excellent example of this can be found in [20].

3D miniaturization of antennas requires detailed knowledge of the operational principles of the antenna. Resonant antenna structures, such as the traditional dipole and loop antenna, are typically narrowband and operate by establishing a portion of the wavelength along the conductor [1]. The resonant characteristic of this category of antenna gives way for higher levels of miniaturization as compared to a traveling wave antenna. A compact loop antenna was measured to have improved performance when incorporating pin loading to introduce the third dimension to the antenna element [21]. This technique forced the current to travel along the length of each pin providing a longer electrical path in the antenna while increasing the efficiency of the antenna from 13% to 82%. For ultra-wideband applications inductive loading of an equiangular spiral antenna was achieved by coils the arms gradually allowing the -15 dB gain point to be miniaturized [22].

This chapter will introduce the main contribution of this work, the periodic spiral antenna (PSA). To explain the operational principles of this antenna a unit cell will be developed and a parametric analysis will be presented. A spiral antenna can be thought of a concentric series of

loop antennas therefore the same miniaturization technique has been applied to a square loop antenna and the performance benchmarked against an un-miniaturized square loop antenna. Since the PSA antenna uses the third dimension for the antenna element a modified cavity was designed to improve antenna parameters, such as return loss, efficiency, and gain, while maintaining the front to back ratio.

4.2. Periodic Spiral Antenna Design

A traditional two arm spiral antenna radiates by exciting a traveling wave along the arms of the spiral with each arm having opposite polarization at the feed point [23]. Radiation occurs when the current of adjacent arms is in phase creating constructive interference in the far-field. This leads to the concept of radiation bands within the spiral antenna where each band creates a loop that is λ_g in circumference. This shows that the high frequency limit is created by the resolution of the inner turns and the low frequency limit is controlled by the outer circumference of the antenna. When applying miniaturization to a spiral antenna it is desirable to decrease the wave velocity in the low frequency portion of the spiral while leaving the high frequency portion unmodified. Ideally this will decrease the low frequency operational point of the antenna while leaving the high frequency operational point intact. Traditionally this is done by designing a tapered substrate that increases in height as it approaches the outer portion of the spiral, concentrating higher levels of dielectric loading at the low frequency region of the spiral.

The Periodic Spiral Antenna is created by orienting each arm normal to the plane containing the spiral and oscillating the arms in the same dimension with the amplitude as a function of angular distance (See Figure 4.1). The shape of the Periodic Spiral Antenna can best be described in cylindrical coordinates by equation (4.1) where is A the Archimedean growth rate and $f(\phi)$ is a function that controls the amplitude growth pattern of the antenna. In Figure 4.

$f(\phi) = B\phi \sin(N\phi)$ where B is the amplitude growth factor and N is the number of oscillations per turn.

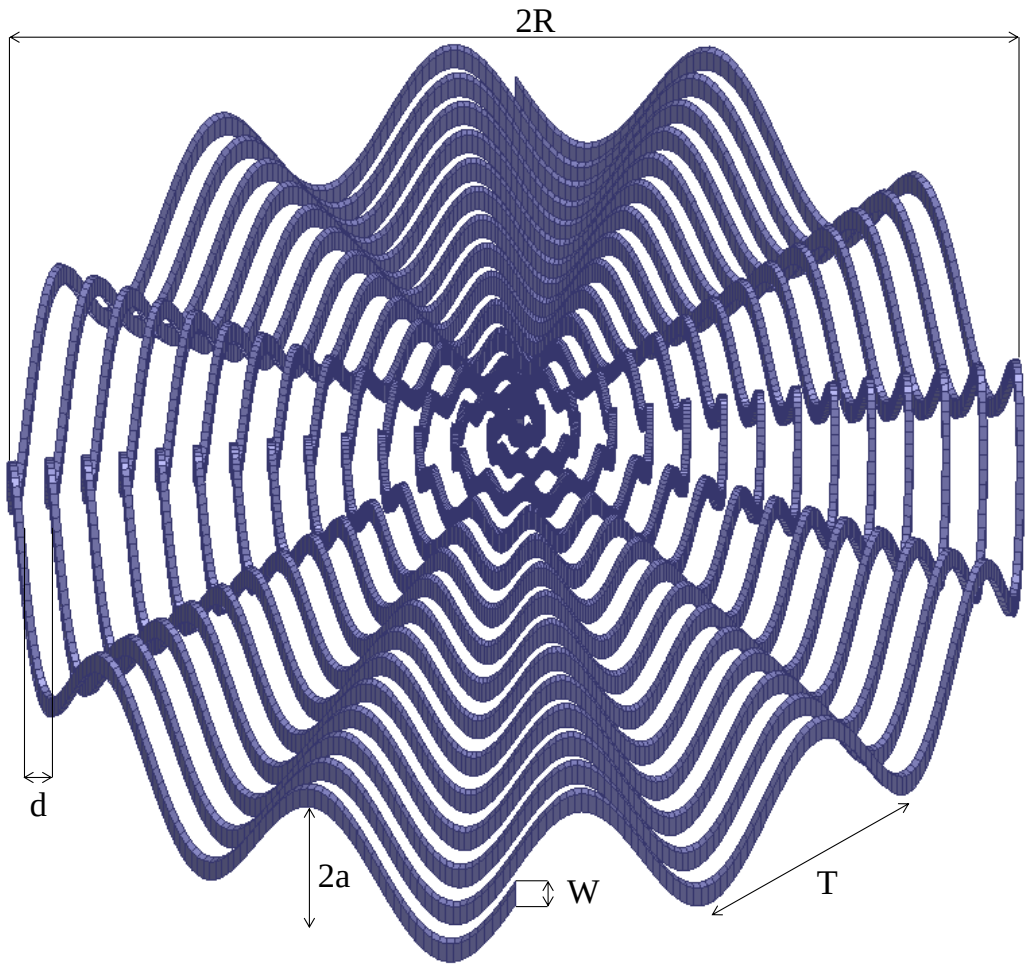

Figure 4.1: Layout of periodic spiral antenna where R is the radius, d is the spacing between conductors, W is the width of the conductor, a is the amplitude of oscillation, and T is the period of oscillation.

$$\vec{r} = A\phi\,\hat{\rho} + f(\phi)\,\hat{z} \tag{4.1}$$

4.3. Parametric Study of Unit Cell

To characterize the contribution of each parameter to the overall antenna miniaturization a unit cell was modeled consisting of a defined length (ΔZ) as shown in Figure 4.2. This unit cell

was used to vary the parameters individually and fit the scattering matrix of the developed equivalent circuit model shown in Figure 4.3. Since coupling between adjacent oscillations on the same transmission line is important the unit cell had to be extracted from a more complicated model [24]. With this method a larger model is simulated consisting of N unit cells cascaded together and another model is then simulated consisting of N-1 unit cells. The transfer matrix of the N model is then divided by the transfer matrix of the N-1 model resulting in an average transfer matrix of a single unit cell. This allows the single unit cell to be more accurately modeled as it is in the antenna. To prove the accuracy of this method and the equivalent circuit model an eigenmode simulation was carried out with HFSS 15.0 and the phase velocity calculated from the results [25]. Since this is known as the most accurate way to simulate phase velocity along a transmission line it was used as the benchmark for comparison to the calculated phase velocity from the inductance and capacitance present in the equivalent circuit model. Comparison results of the two methods are shown in Figure 4.4. This shows that the equivalent circuit model corresponds well with the eigenmode simulation with the deviation increasing with amplitude. The increasing error is an effect of the physical model becoming dispersive as the amplitude is increased. Figure 4.4 shows that the velocity of propagation is reduced by a factor of 3 compared to the original value at an amplitude of 7 mm.

The Archimedean growth rate (a) controls the spacing between arms and therefore the amount of capacitance per unit length along the arm. Due to the arms being oriented parallel to the z-axis the capacitive coupling between arms in increased. Orienting the arms in this direction also allows for the Archimedean growth rate to be decreased further increasing the capacitance and therefore miniaturization. This configuration of a spiral antenna is studied further in [26].

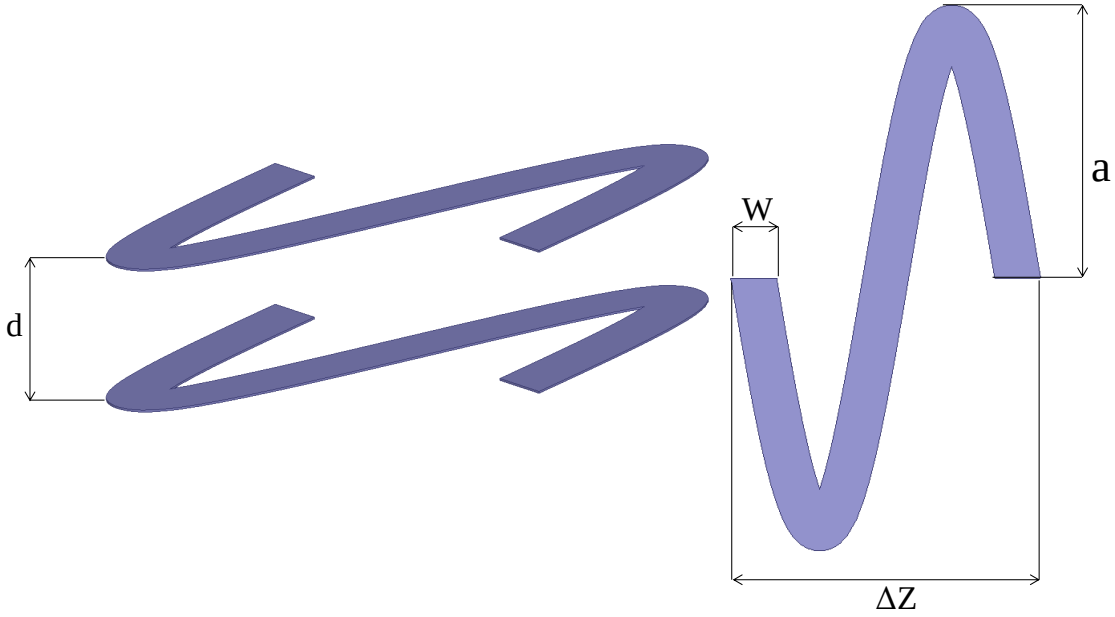

Figure 4.2: Unit cell developed for parametric analysis

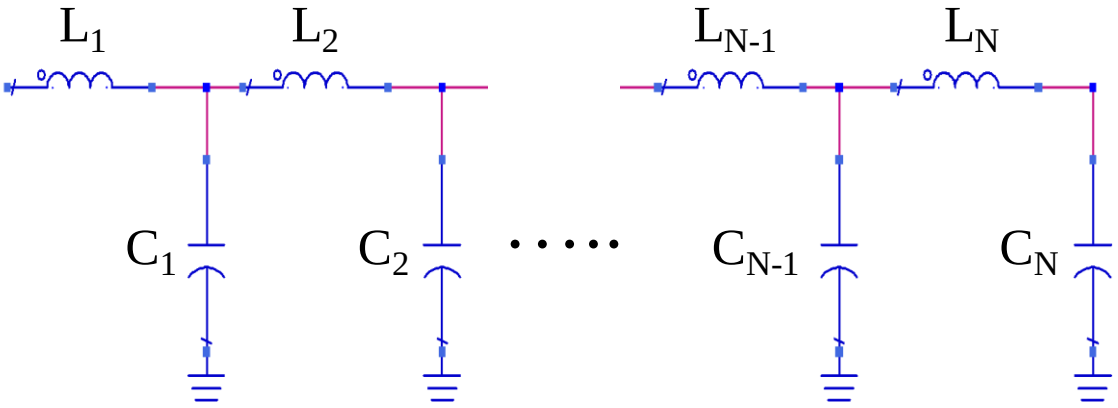

Figure 4.3: Equivalent circuit model assuming PEC and lossless medium

The amplitude growth rate (B) and the number of oscillations per turn (N) affect the amount of effective inductance and capacitance that is added. The number of oscillations per turn can be thought of as the parameter that controls the maximum amount of available inductance and capacitance while the amplitude growth rate controls the actual values added. This means that for a specified, achievable, miniaturization factor there are two sets of parameters, an

amplitude growth rate and number of oscillations per turn, which will yield the same result. One set will contain a larger amplitude growth rate factor with a lower number of oscillations and the other will contain a lower amplitude growth rate factor with a higher number of turns. To observe how inductance and capacitance change as a function of amplitude and period the unit cell was used with the period, *T*, was set to 6.28 mm and 12.57 mm. At each period the amplitude was swept from 0 mm to 12 mm. Results of this study can be seen in Figure 4.5. The benefit of choosing the combination with a smaller amplitude growth factor is that the overall height of the antenna will be smaller. In situations where the antenna will be backed by a shallow cavity and there is a restriction on overall height this option will keep the antenna farther away from the cavity bottom reducing unwanted effects in the antenna parameters. The second combination will have a smaller number of oscillations but a larger overall height profile.

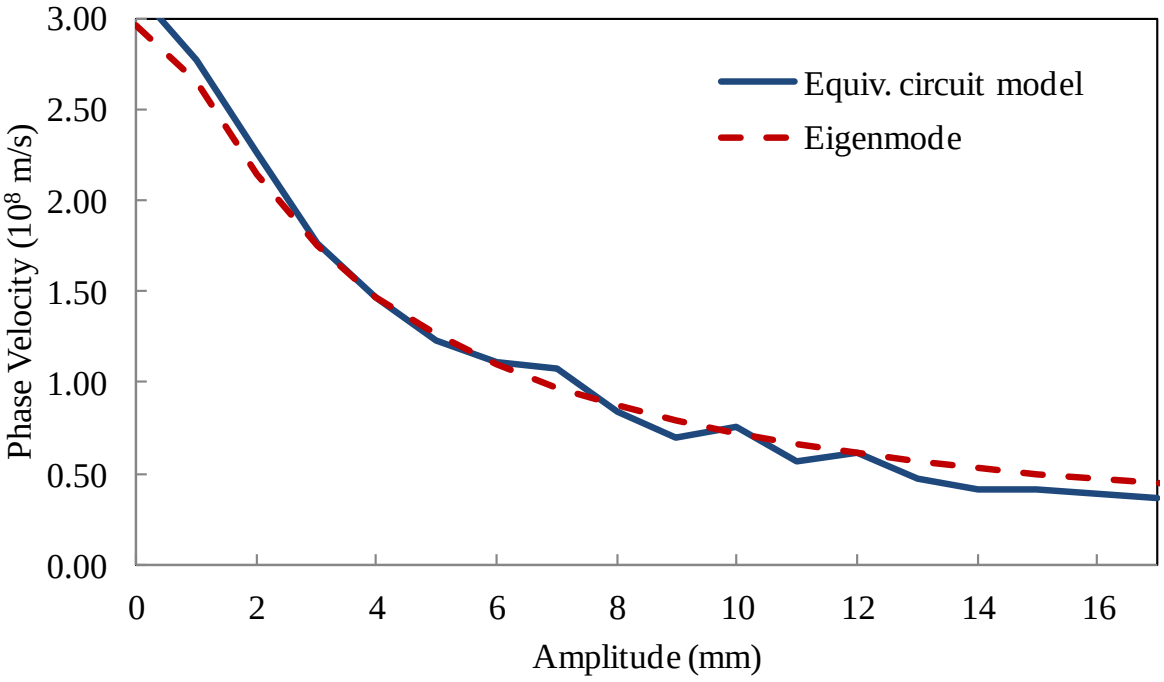

Figure 4.4: Phase velocity as a function of amplitude (*a*) with a conductor spacing (*d*) of 100 mils. This graph shows the phase velocity calculated from the proposed equivalent circuit model and the eigenmode simulation.

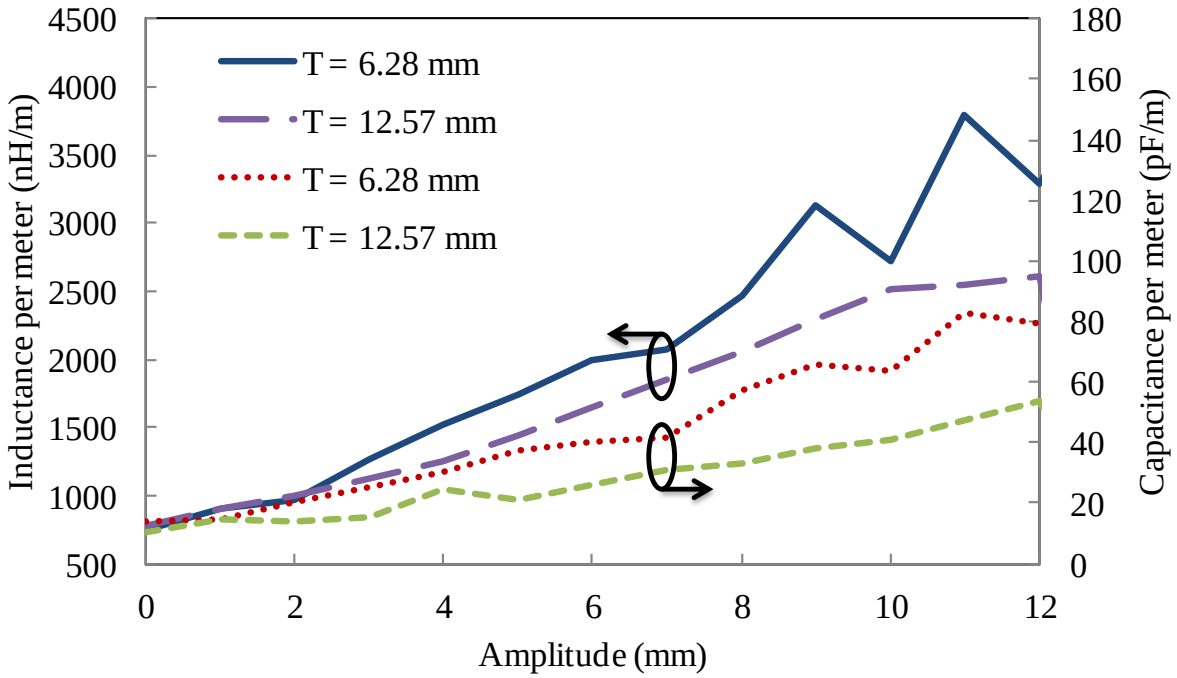

Figure 4.5: Inductance and capacitance per meter as a function of amplitude (*a*) with a period (*T*) of 6.28 mm and 12.57 mm

The phase velocity along the arms of the antenna is an indicator to the amount of miniaturization achieved and is a combination of the capacitance and inductance present. Since a spiral antenna is not a resonant antenna the miniaturization factor is not equal to the reduction in phase velocity. To show this an eigenmode simulation was carried out which held the spacing between the conductors at 2.54 mm (100 mils) and varied the amplitude from 0 mm to 7 mm. Then a periodic spiral antenna was simulated with the same spacing and the maximum amplitude on the outer arm ranging between the same values. This PSA model was then compared to a planar Archimedean spiral and the 0 dB gain point was used to calculate a miniaturization factor. Figure 4.6 shows the phase velocity and the corresponding miniaturization factor. When applying a large amount of miniaturization the return loss of the antenna begins to degrade resulting in a smaller shift in the 0 dB realized gain point per incremental increase in amplitude.

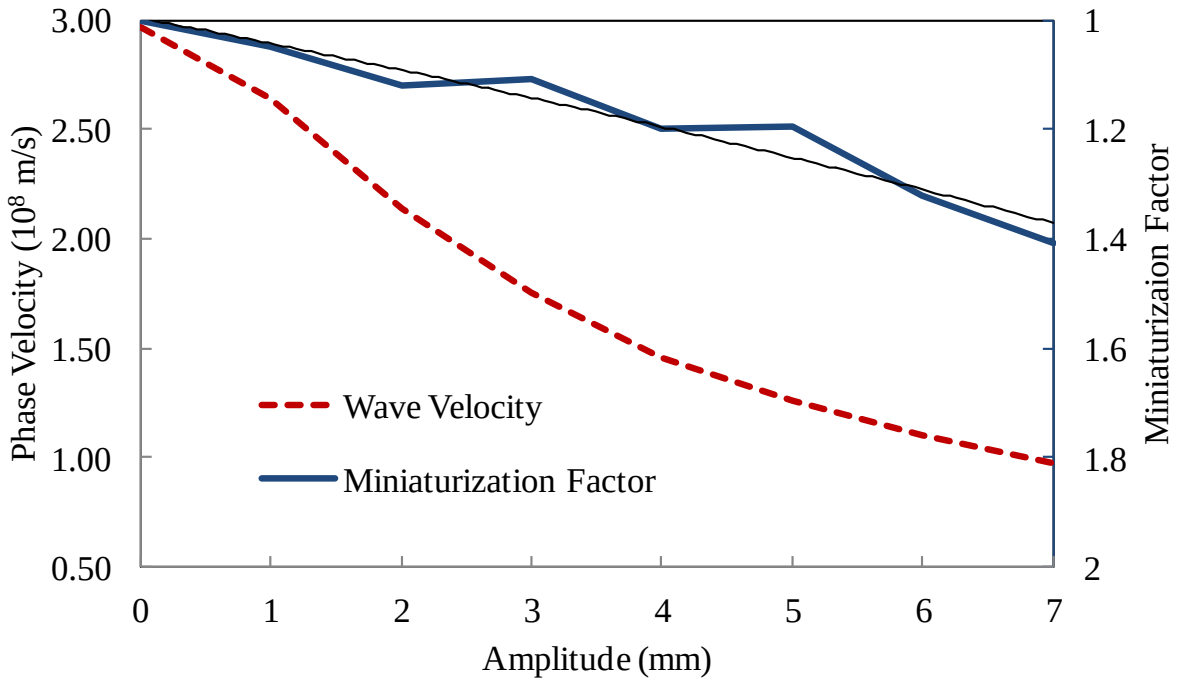

Figure 4.6: Velocity of propagation calculated from the unit cell model and simulated miniaturization factor versus outer amplitude.

4.4. Applications of Three Dimensional Miniaturization

It has been shown that better use of the radian sphere containing the antenna will increase the overall efficiency of an antenna [20] [21]. To achieve the best performance in terms of miniaturization factor and antenna parameters the design must utilize all three dimensions. In this section a parametric study will be presented on a loop antenna that has been miniaturized using this technique. A loop antenna was chosen because a spiral antenna can be thought of as a concentric series of loop antennas creating the radiation bands within the spiral [27]. This study uses the square loop antenna shown in Figure 4.7 where L is the side length, a is the amplitude, and T is the period of oscillation.

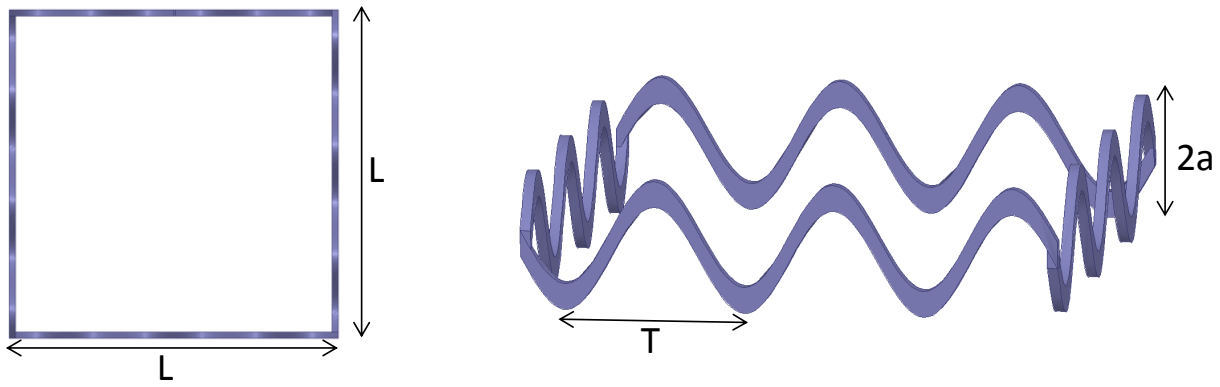

Figure 4.7: (Left) Top view and (Right) profile view of 3D miniaturized square loop antenna.

To quantify the miniaturization achieved a full wave simulation was carried out using HFSS 15.0 and the antenna parameters were calculated. Three different styles of loop antennas were designed to resonate at 2.4 GHz in free space with each design using PEC conductors. The first antenna was a planar loop, the second was a planar meandered loop, and the third was a three dimensional meandered loop antenna. Each model was fed by a lumped port matched to the antenna's input resistance at resonance. For this study a random overall height of 6.35 mm (250 mils) was chosen for the three dimensionally miniaturized antenna and the length, *L*, and period, *T*, were varied. For simplicity the three dimensional meandered loop antenna was only meandered in the z-dimension while keeping the broadside of the antenna a square. For comparison purposes two 3-D meandered loop antennas were analyzed: model A was made with the same length as the planar meandered loop, while model B had a decreased length (L) while decreasing the period (T) to maintain a resonance at the design frequency and show the extent of achievable miniaturization. Model B was miniaturized until the return loss bandwidth percentage dropped below 1%. A layout of each design can be shown in Figure 4.8. It should be noted that model B could potentially get volumetrically smaller if meandering in the x-y plane was employed on this design.

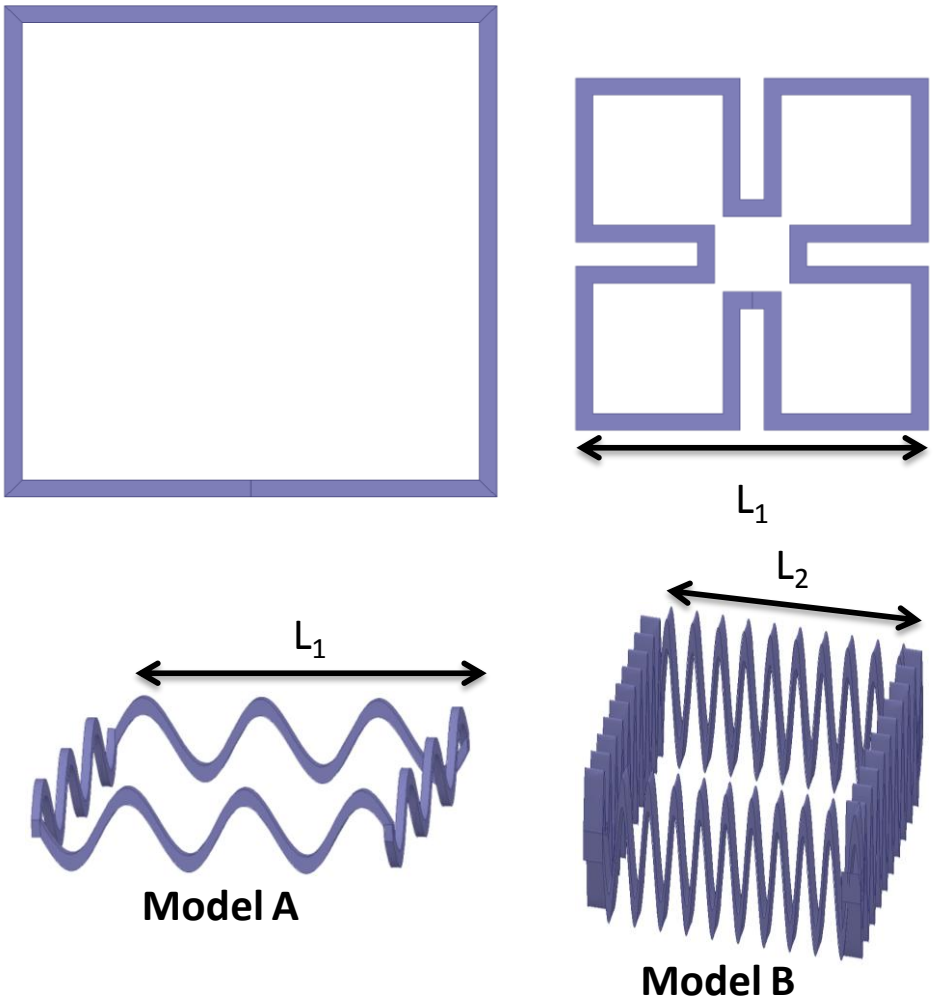

*Layout not to scale

Figure 4.8: Layout of square loop antenna (top left), planar meandered loop (top right), 3D miniaturized loop antennas (bottom)

Return loss and realized broadside gain of each antenna model are shown in Figure 4.9 and Figure 4.10. This data shows that for the planar meandered loop antenna the bandwidth where S11 ≤ -10 dB is 135.3 MHz with a broadside gain of 3.1 dB with a 3 dB bandwidth of 402.8 MHz. This model has a 27% smaller footprint than the original loop antenna. In comparison model A exhibited a 223.9 MHz return loss bandwidth with a broadside realized gain of 2.85 dB and a 3 dB bandwidth of 836.7 MHz. Compared to the planar meandered model this design had a 3 dB gain bandwidth that was 2.1 times larger with a 0.21 dB decrease in peak realized gain due

to a slight pattern reshaping. Model B boasted the smallest footprint of any design measuring a length of 8.64 mm (340 mils). This design resulted in a return loss bandwidth of 17.3 MHz, a peak gain of 2.09 dB, and a 3 dB realized gain bandwidth of 52.7 MHz. A summary of these results can be seen in Table 4.2.

Table 4.2. Simulation study results of different miniaturization techniques

Loop Style	Side Length (mils)	Surface Area Reduction (%)	S11 ≤ -10 BW (MHz)	Peak Gain (dB)	3dB Gain BW (MHz)
Traditional Square	1430	0.00%	358.5	3.68	1698.8
Planar Meandered	1036	47.50%	135.3	3.063	494.2
3D Meandered (Model A)	1036	47.50%	223.9	2.85	836.7
3D Meandered (Model B)	340	94.35%	18	2.09	54.4

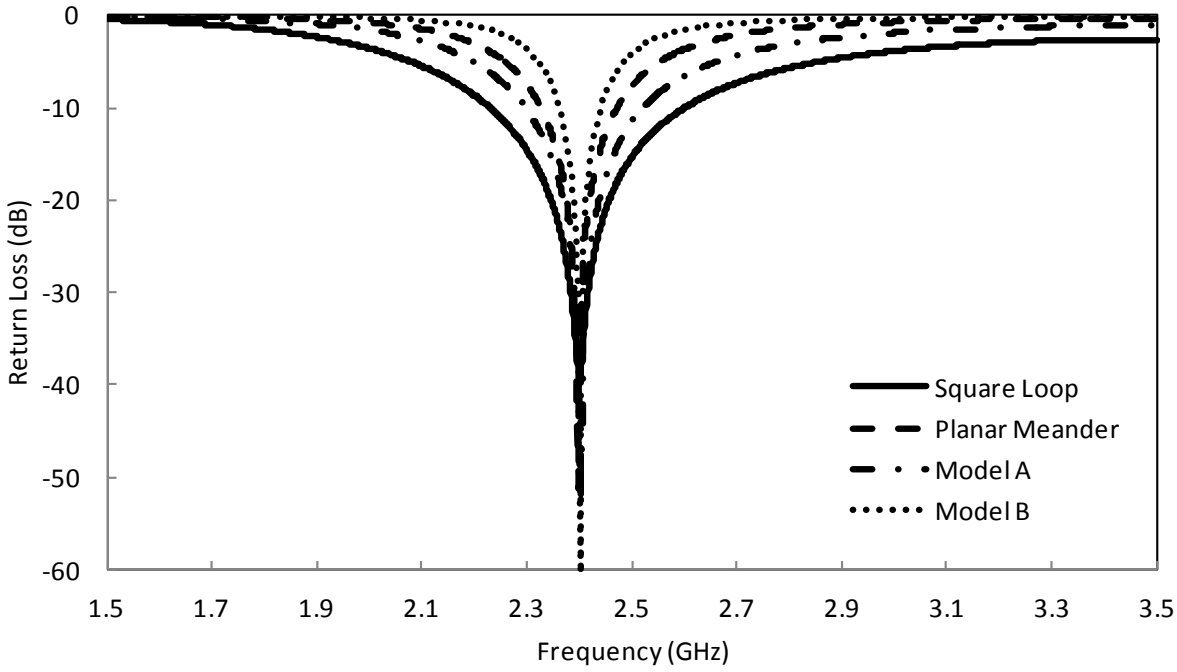

Figure 4.9: Return loss matched to the antennas input resistance at resonance

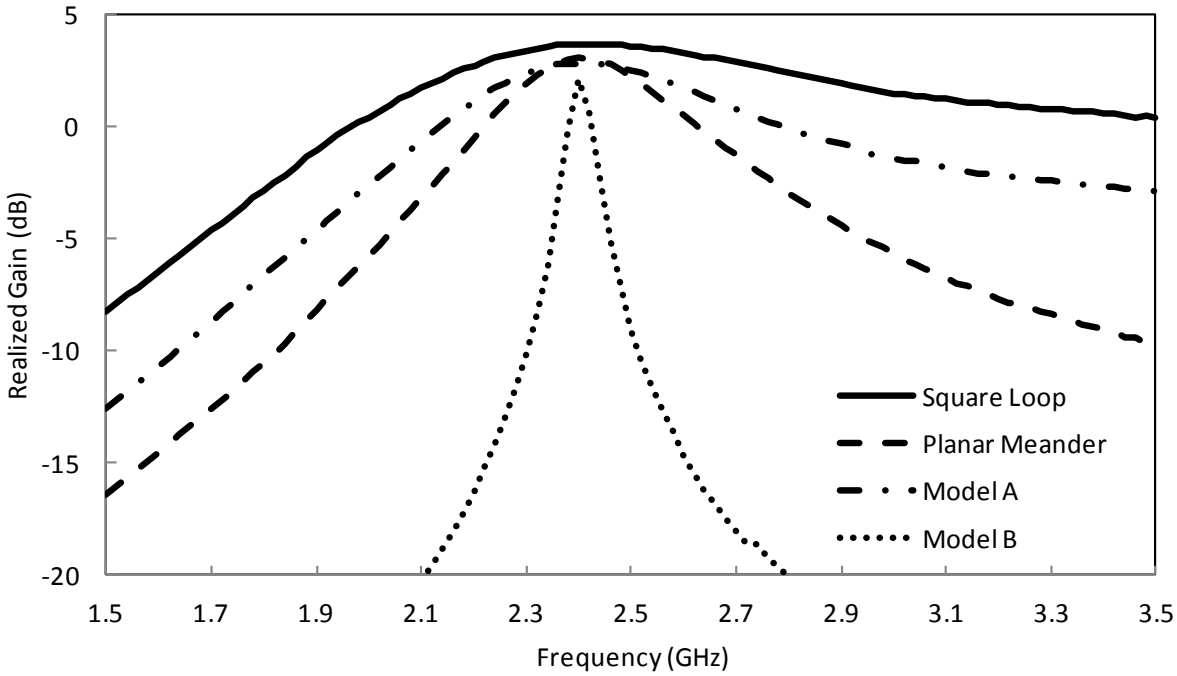

Figure 4.10: Realized broadside gain of each loop antenna model

4.5. Periodic Spiral Antenna Amplitude Growth Profile

The amplitude growth rate of the periodic spiral antenna determines the overall height of the antenna. The height of the antenna, along with the period of oscillation, at each radiation ring determines the amount of miniaturization. When employing dielectric loading it is common practice to employ a tapered profile which introduces higher levels of loading on the lower frequency regions of the spiral leaving the high frequency regions unaltered [28]. The layout shown in Figure 4.1 implements a linear amplitude growth profile which was characterized in section 4.3. To investigate the effect of making the amplitude growth profile non-linear a model was designed to maintain the maximum amplitude of the periodic spiral antenna and vary the method of growth. Figure 4.11 shows different amplitude growth profiles as a function of the radius of the spiral. Here a linear growth profile is compared against an exponential growth profile and an arctangent growth profile. The goal is to investigate how the level of

miniaturization that is applied to each radiation ring affects the wideband performance of a spiral antenna.

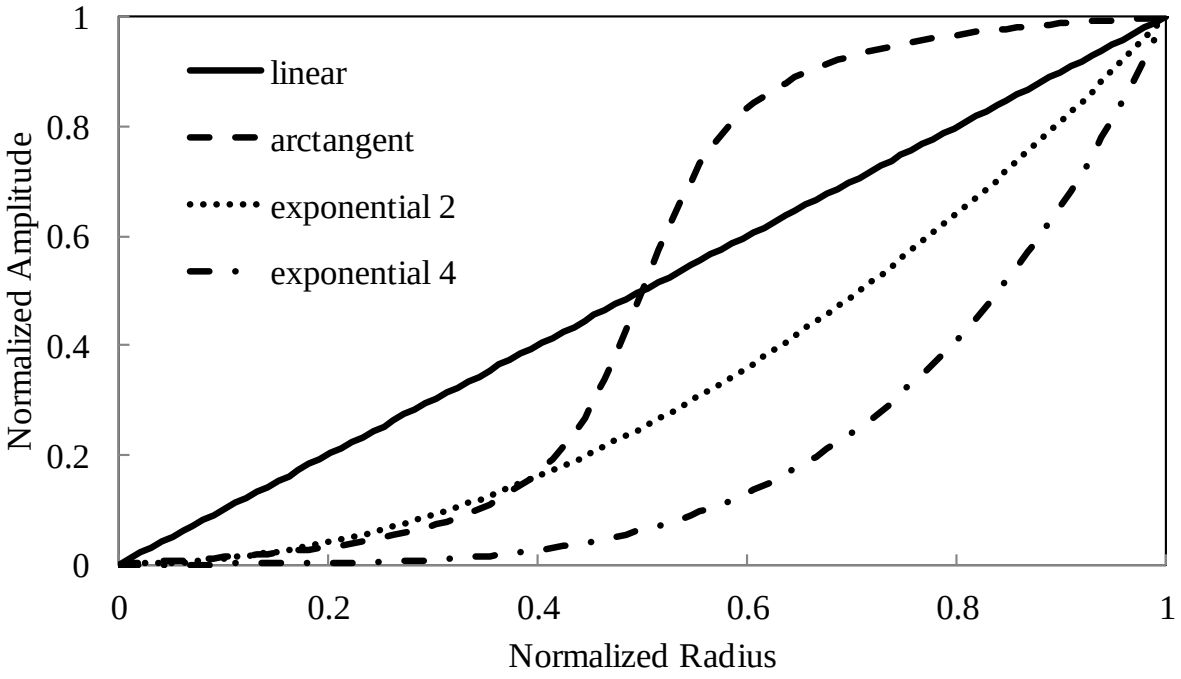

Figure 4.11: Cross section showing different amplitude growth profiles for the periodic spiral antenna

As seen in Figure 4.12 and Figure 4.13 the arctangent growth curve results in minimal variation in realized broadside gain however it shows degradation in the axial ratio across the frequency band. The length of the antenna arm is also increased by 2.1% compared to the linear amplitude growth profile resulting in no benefit to choosing this growth profile. Equation (4.2) describes the shape of the periodic spiral antenna with an exponential amplitude growth rate where x is the exponential factor of growth. Comparing the arm length of a linear growth profile to an exponential factor (x) of 2 results in a 21% decrease while an exponential factor of 4 results in a 34% reduction. Referring again to Figure 4.12 and Figure 4.13 it can be seen that the realized broadside gain is maintained using the exponential growth profile compared to a linear

growth profile. It can also be noted that the exponential growth profile shows improvements in axial ratio at higher frequencies. This can be explained by investigating the flatter aperture of the antenna in the high frequency region. Any physical height difference of the antenna element in the radiation band will cause a phase shift in the far-field of the antenna causing degradation in axial ratio. At exponential factors above 4 the maximum achievable miniaturization factors starts to degrade. The increase in operational frequency can be attributed to the amplitude growing too rapidly causing reflections along the arms.

$$\vec{r} = A\phi\ \hat{\rho}\ + B\phi^{x}\sin(N\phi)\,\hat{z} \tag{4.2}$$

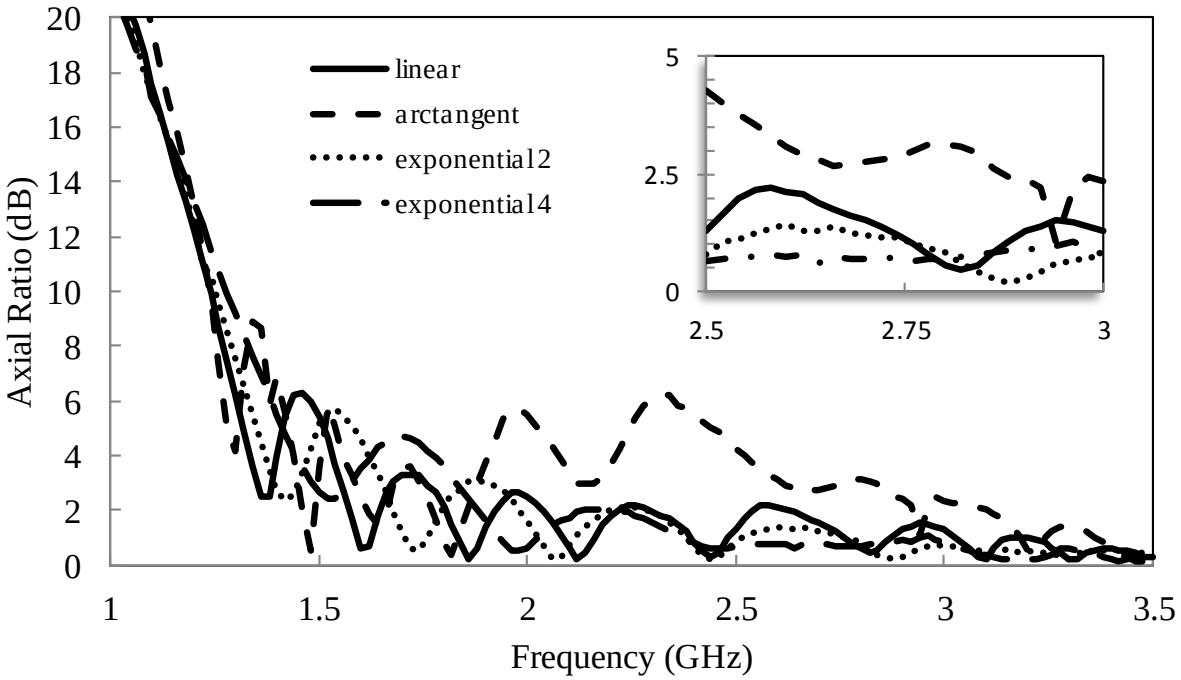

Figure 4.12: Axial ratio for different amplitude growth profiles

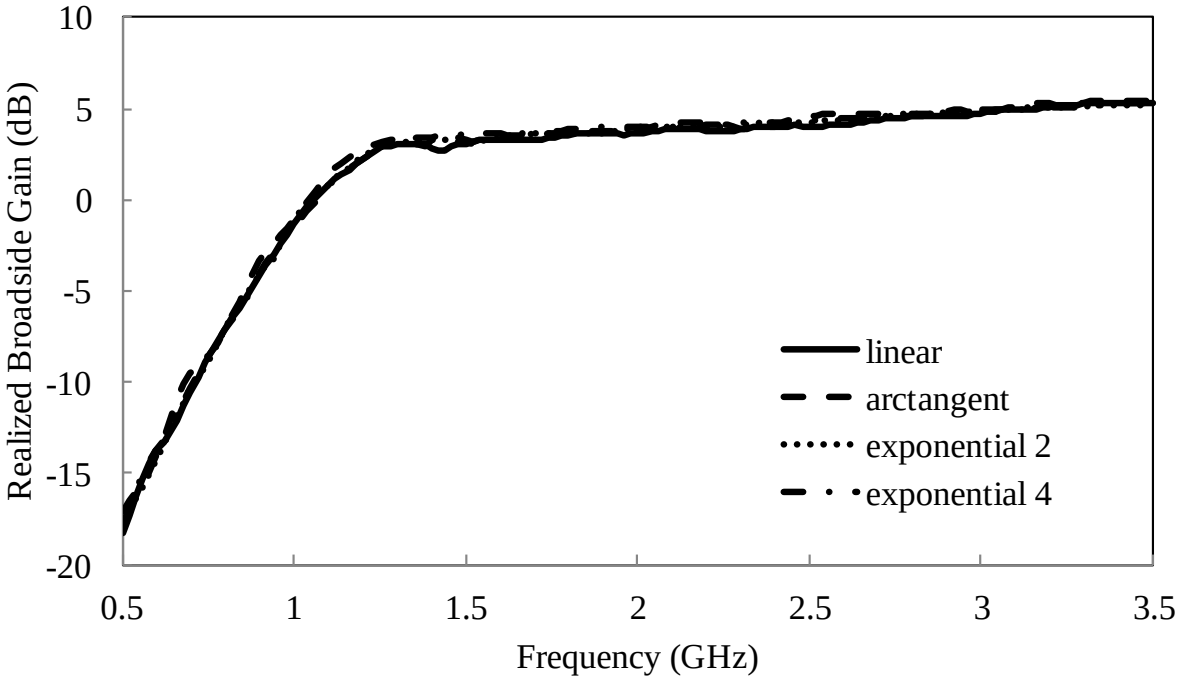

Figure 4.13: Broadside axial ratio for different amplitude growth profiles

4.6. Cavity Design

In applications where unidirectional radiation is desired a cavity is often used to suppress the back lobe level. When using an electrically shallow cavity the wideband characteristics inherent to a spiral antenna deteriorate. This degradation occurs because the waves reflected off the cavity have a reverse direction compared to the antenna element causing undesired effects in the far field [28]. This becomes evident with the increase in axial ratio and return loss. To remedy this studies have been done that add a lossy ring around the outside walls of the cavity to absorb energy present at the tip and reduce reflections [29]. Optimization of the shape of the absorbing ring can improve the reduction in efficiency while maintaining improved axial ratio and return loss. Other methods such as using an EBG reflector around the spiral have shown benefits in restoring the performance of a spiral antenna but require a larger footprint to implement [30].

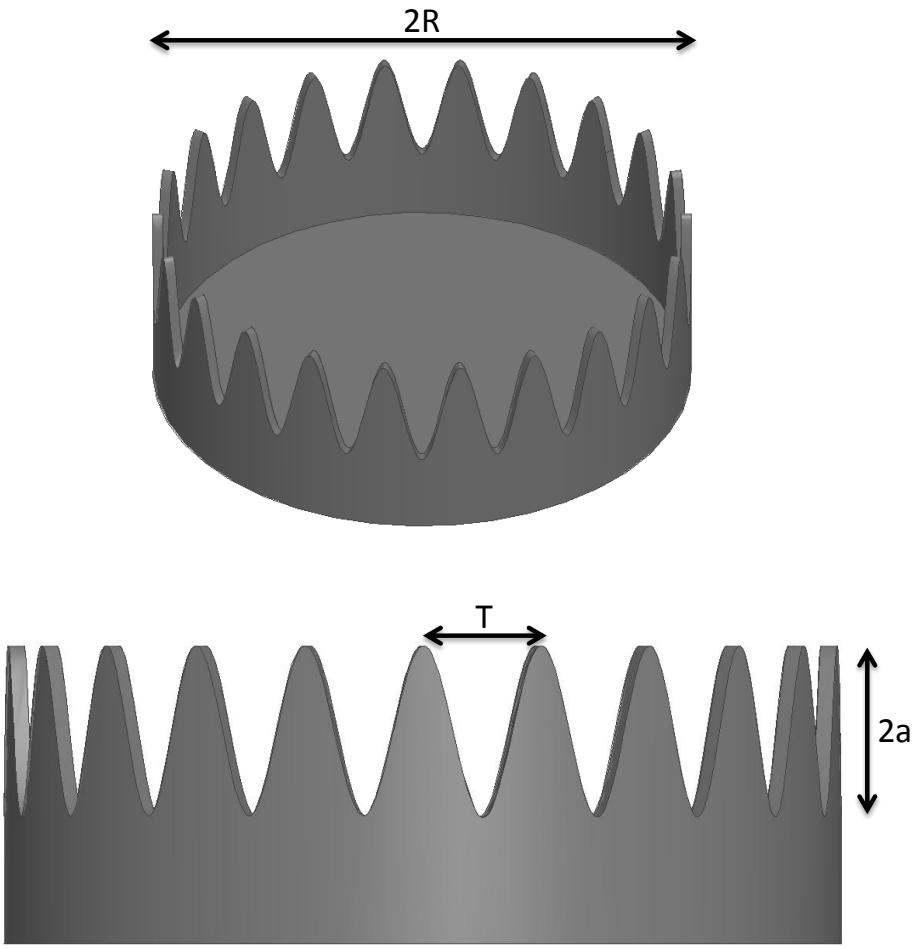

Figure 4.14: Layout of the cavity design for the PSA antenna

For the periodic spiral antenna the distance between the arms of the antenna and the sidewalls of the cavity varies. The sinusoidal valleys of the antenna element will get closer to the cavity walls and can cause power to be transferred to the grounded cavity. To remedy this effect the sidewalls of the cavity were modified to have the same sinusoidal shape as the antenna element, shown in Figure 4.14. It was discovered through simulation that by implementing this sinusoidal shape on the cavity improvements in the return loss and gain were obtained with little sacrifice in the front to back ratio. Furthermore, the amplitude of oscillation on the sidewalls of the cavity can be increased to improve return loss and broadside gain. Figure 4.15 through Figure

4.18 show the effect of maintaining the same distance between the antenna and the cavity walls but adjusting the amplitude of oscillation on the cavity walls (*a*) between 4.3mm (roughly equal to the amplitude of the fabricated antenna) and 8.1 mm. It can be seen from Figure 4.15 that the front to back ratio improves when the amplitude (*a*) is increased on the cavity walls. The broadside gain, shown in Figure 4.16, is improved by 3 dB at 800 MHz while the high frequency gain is maintained. This increase is due to the return loss improving as the amplitude of the cavity is increased (see Figure 4.17). Due to the effect of portions of the cavity being further from the antenna it is expected that the efficiency will increase in the low frequency portion of the antenna, as shown in Figure 4.18. This efficiency increase is due to this section being farther from the cavity walls.

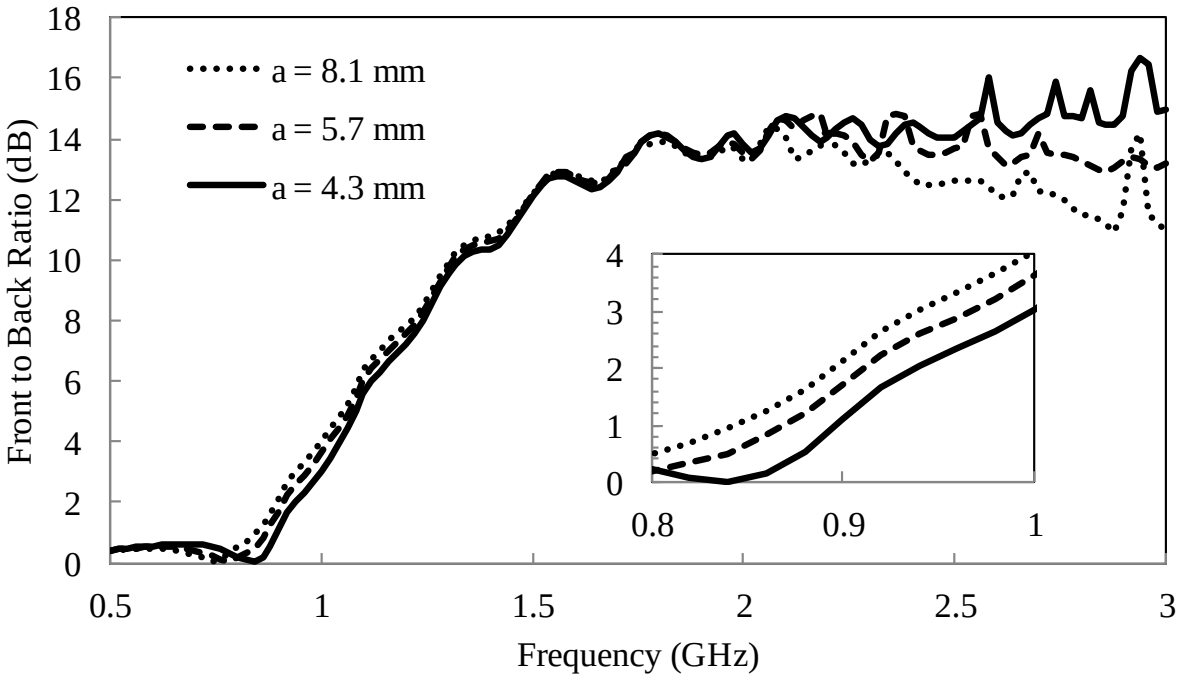

Figure 4.15: Front to back ratio of cavity-backed periodic spiral antenna with different amplitudes of oscillations on the cavity walls

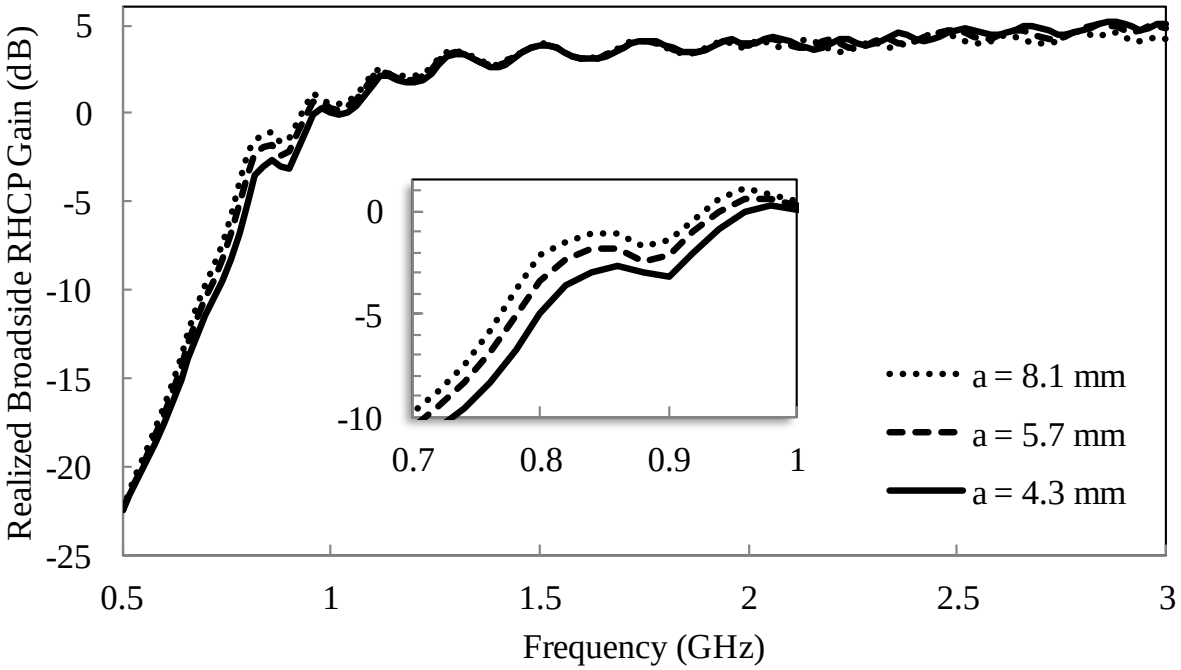

Figure 4.16: Broadside realized gain of cavity-backed periodic spiral antenna with different amplitudes of oscillations on the cavity walls

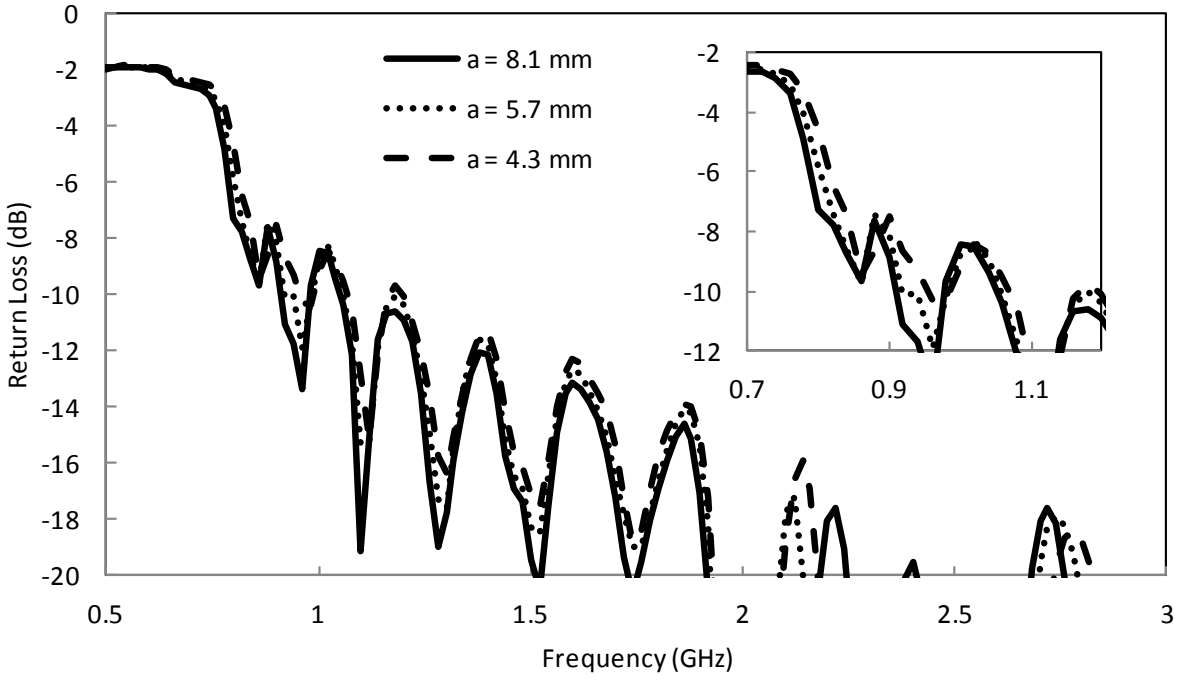

Figure 4.17: Return loss of cavity-backed periodic spiral antenna with different amplitudes of oscillations on the cavity walls

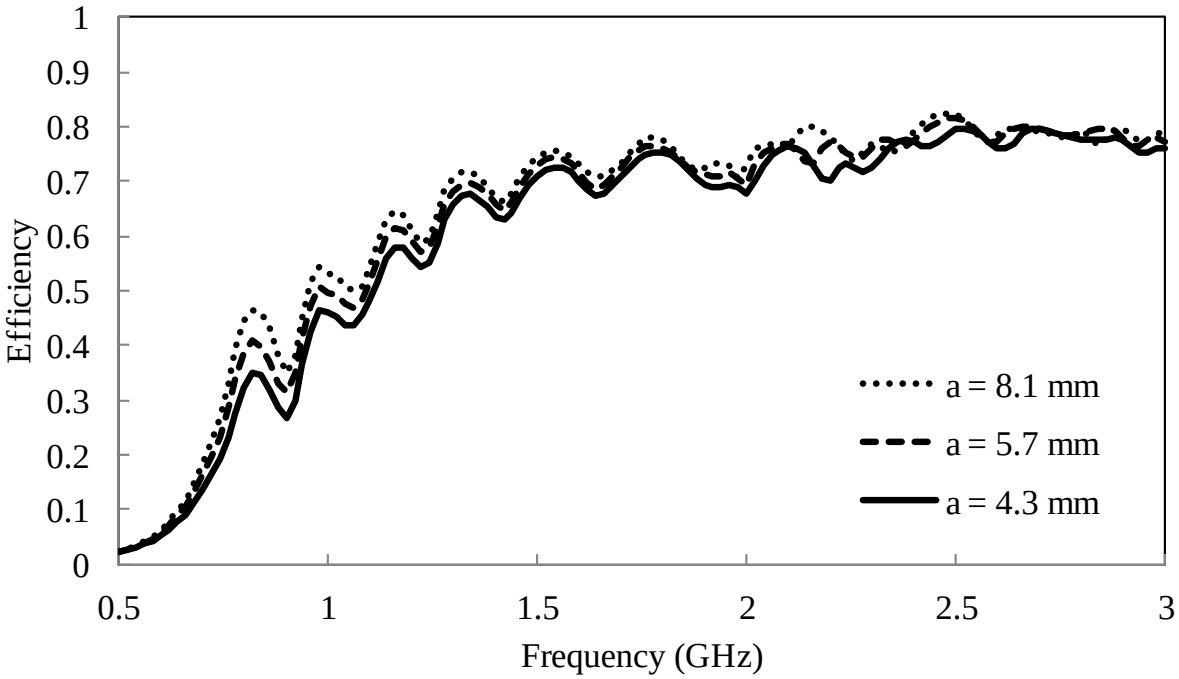

Figure 4.18: Efficiency of cavity-backed periodic spiral antenna with different amplitudes of oscillations on the cavity walls

4.7. Measured Results

The substrate for the PSA antenna was printed with a Fortus 400mc using ULTEM [31]. ULTEM has shown to have low-loss and RF performance comparable to high quality microwave laminates [32]. Additive manufacturing was chosen due to the ease of creating the 3-D features used in the PSA antenna. The top of the substrate contained a groove that was meant to guide the 0.406 mm radius copper wire used to form the antenna element. This process was used to fabricate two different PSA models: a linear growth profile (shown in Figure 4.19) and an exponential growth profile (shown in Figure 4.20). Each model had a diameter of 3" and a height of 1.5" measured from the bottom of the cavity to the top of the substrate. Equation (4.3) was used to design the linear growth profile and equation (4.4) was used for the exponential growth profile. An exponential factor of 3 was chosen since this reduces the wire length by 29.5% and a higher exponential value starts to diminish the achieved miniaturization factor. To feed both

antenna models a tapered balun was fabricated on Rogers RO4360G2. The balun was used to transform the input impedance of the antenna to 50 Ω and change the electric fields from the unbalanced coaxial feed to the balanced field distribution required for the antenna. Measured performance was achieved by placing two baluns back to back and comparing the simulated return loss against the measured return loss. Agreement between the simulated and measured return loss proved the accuracy of the simulator which was then used to simulate the s-parameters of the single ended balun. A layout of the balun and s-parameters can be found in Appendix A.1.

Figure 4.19: Fabricated model of sinuous cavity backed PSA antenna utilizing a linear growth profile

$$\vec{r} = A\phi\,\hat{\rho} + B\phi\,sin(N\phi)\,\hat{z} \tag{4.3}$$

where $A = 0.08\,cm, B = 0.09\,mm, N = 22, 0 < \phi < 14\pi$

The return loss of each model was measured with an Agilent 8720E vector network analyzer. The return loss of the linear growth model is compared against the exponential growth model in Figure 4.21. The improvement exhibited by the exponential growth model between 1.3 GHz and 2 GHz can be attributed to the wire better conforming to the substrate reducing reflections along the wire in this frequency region. Figure 4.22 shows the measured broadside RHCP gain of both models with good correlation throughout the operational band with the linear and exponential growth profiles having a 0 dB gain point at 917 MHz and 880 MHz, respectfully. Radiation patterns of each model at 1.5 GHz and 2.4 GHz can be seen in Figure 4.23 showing good correlation in total gain between the two models.

Figure 4.20: Fabricated model of sinuous cavity backed PSA antenna utilizing an exponential growth factor of 3

$$\vec{r} = A\phi\ \hat{\rho}\ + B\phi^{x}\ sin(N\phi)\ \hat{z} \tag{4.4}$$

where $A = 0.08\ cm, B = 46.53\ nm, x = 3, N = 22, 0 < \phi < 14\pi$

To show the effects of using a cavity the exponential growth model was measured without the cavity (dielectric loaded), with a flat cavity along the bottom of the substrate (back cavity), and a full sinuous cavity (as shown in Figure 4.20). Return loss measurements are shown in Figure 4.24. Comparing the return loss measurements of the model with the back cavity and the full sinuous cavity will show the improvements made by adding the sinuous side walls to the cavity. For example, at 860 MHz the return loss of the back cavity and full cavity models were 5.26 dB and 10.93 dB, respectfully, showing an improvement of 5.67 dB. The improvement in return loss when adding the sinuous side walls to the cavity also comes with an improvement in the front to back ratio, which was proven through full-wave simulation in section 4.6.

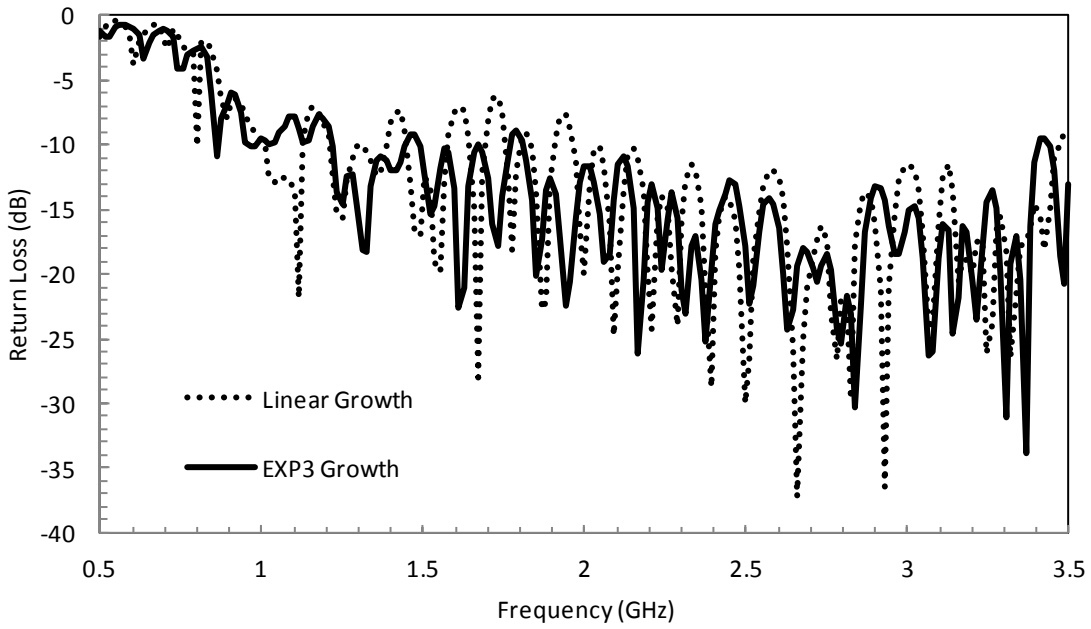

Figure 4.21: Return loss of sinuous cavity backed PSA antenna with linear growth and exponential growth factor of 3

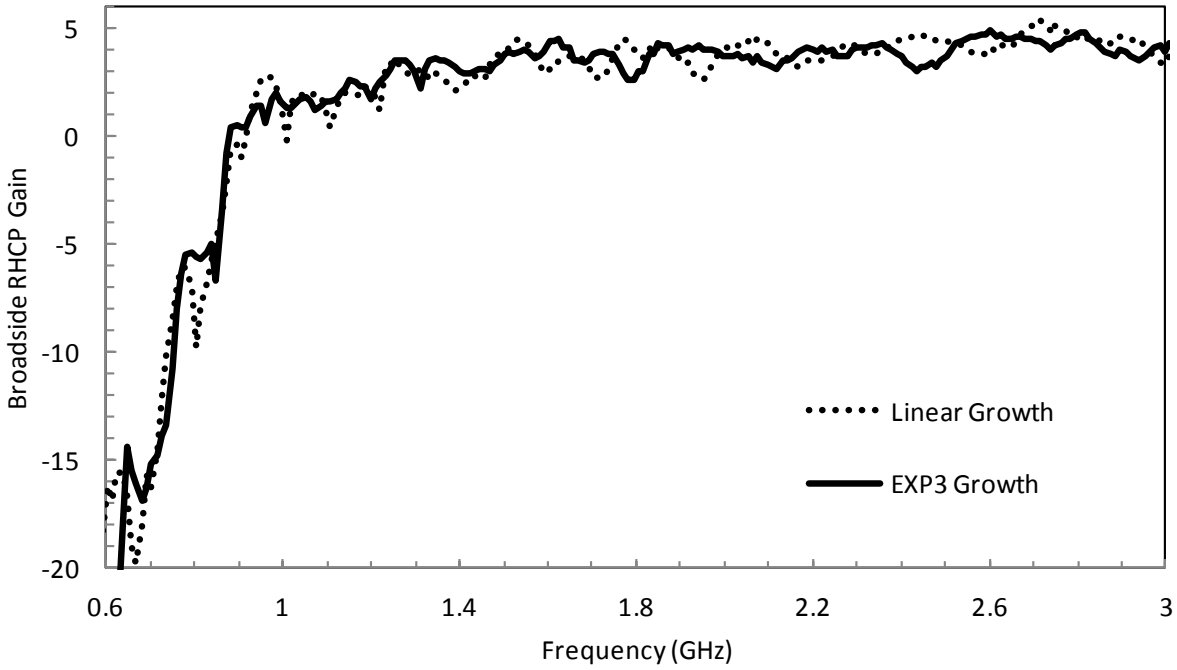

Figure 4.22: Measured broadside RHCP gain of sinuous cavity backed PSA antenna with linear growth and exponential growth factor of 3

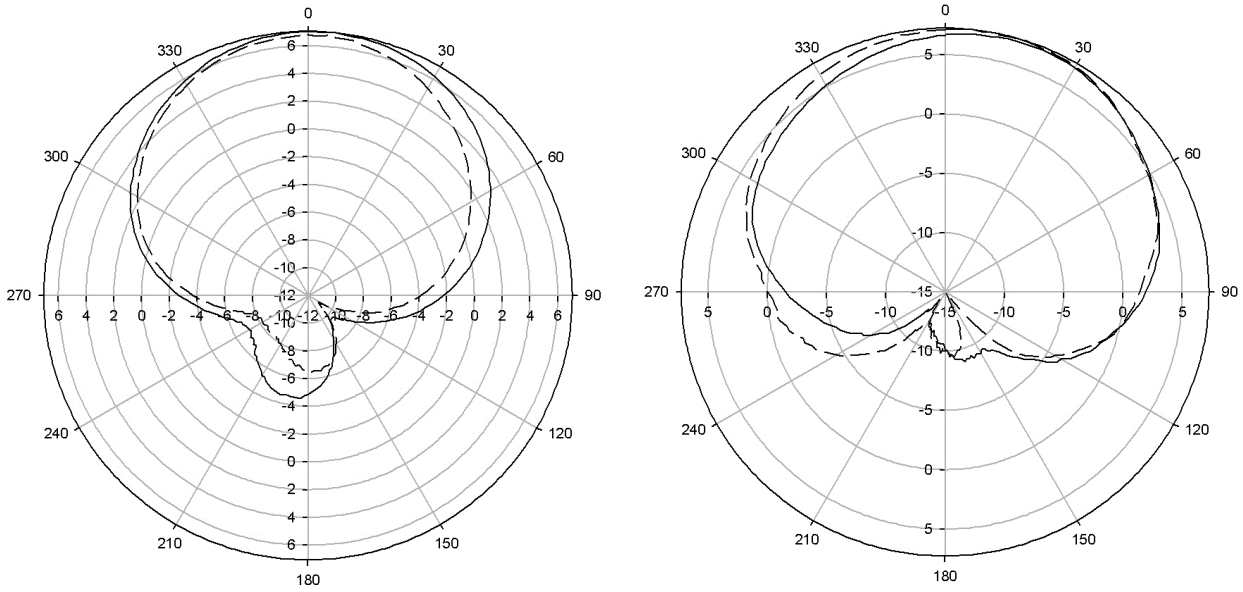

Figure 4.23: Radiation pattern comparison for linear model (dashed line) and exponential model (solid line) at 1.5 GHz (Left) and 2.4 GHz (Right)

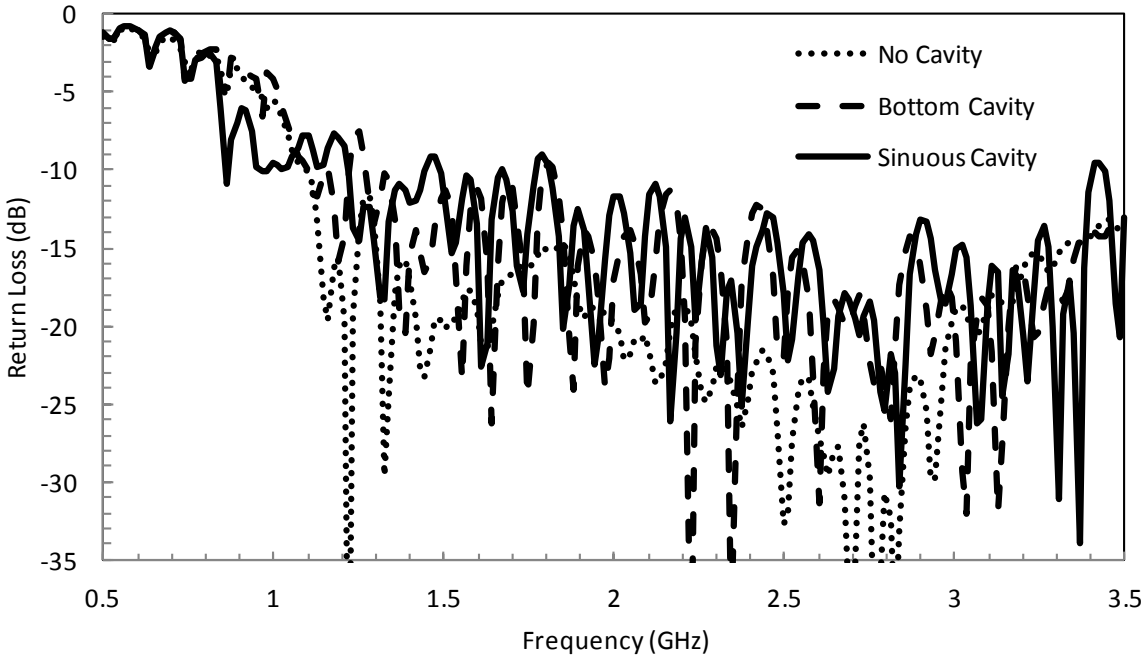

Figure 4.24: Return loss of PSA antenna with exponential growth factor of 3 using different cavity configurations

4.8. Conclusion

This chapter presented the periodic spiral antenna along with an equivalent circuit model to characterize the effect of varying each parameter in the antenna. To prove the effectiveness of meandering in the z-dimension a loop antenna was modeled and the size and performance benchmarked against traditional planar miniaturization techniques. Further improvement of the PSA antenna was achieved by employing an exponential growth profile which reduced the material and weight of the structure while improving return loss and axial ratio. The measured radiation patterns of both fabricated models also show consistency when changing the amplitude growth profile.

Chapter 5: Conclusion

5.1. Summary

This thesis covered basic antenna design by introducing theory of operation and showing some simple examples of how to reduce the physical dimensions of an antenna. The limit of miniaturization was presented through Chu's theory which compares the quality factor of antenna to the sphere surrounding the structure. The power handling capabilities of RF structures, whether they are microstrip or antenna designs, were covered along with some guidelines for decreasing thermal generation at any given power level. In general the steady-state temperature of a RF structure can be decreased by using wider lines (lower permittivity), low-loss substrates, and high thermally conductive materials.

The introduction of the periodic spiral antenna (PSA) presented an equivalent circuit model which can be leveraged to understand the effect of each design parameter. This equivalent circuit model was used to quantify changes in inductance and capacitance as a function of changing dimensions. From here a comparison of a PSA antenna showed that the highest achievable miniaturization factor investigated was 1.4 at an amplitude of 7mm, using the 0 dB gain point. Amplitudes above 7 mm were not investigated due to the specifications of this project but expect to see higher levels of miniaturization. Further improvements in the weight and performance of the PSA antenna were achieved by incorporating a non-linear growth profile to the antenna. More specifically, an exponential growth factor of 3 allowed the wire to be reduced by 29.5% while improving the axial ratio, return loss, and broadside gain. Radiation patterns of both the

linear and exponential growth models show consistency which proves the performance as a radiator.

5.2. Future Work

The models fabricated in this thesis used 3D printing to manufacture the substrate of the antenna. The material chosen for the substrate was ULTEM due to the favorable high frequency performance as well as the temperature handling capabilities. Current 3D printable low-loss materials available for RF applications are limited and have a permittivity below 3.5. Further development of high permittivity, low-loss materials could provide additional miniaturization on the presented designs. With a higher permittivity substrate the diameter as well as the height of the antenna could be reduced or the performance can be improved with the current dimensions. Ongoing research in this area includes mixing currently available thermoplastics with low-loss ceramics to increase the permittivity. Challenges of this approach lie in maintaining the mechanical properties while mixing materials.

The presented models used 20 AWG copper wire to form the antenna element increasing fabrication time and decreasing reliability between units. To further improve manufacturability of the PSA antenna additive manufacturing can be used to print the antenna element. Preliminary simulation studies show the decreased conductivity of a printed conductor will cause minimal change in realized RHCP gain. This is due to the improved return loss and axial ratio across the band which can be attributed to less power present at the tips of the spiral reducing reflections. A challenge to implement this manufacturing method is the ability to print a conductor as thick as the copper wire used (diameter = 0.812 mm).

References

[1] Balanis, Constantine A. “Antenna Theory: Analysis and Design.” Hoboken, N.J: Wiley-Interscience, 2005.

[2] Chen, Chun-Chyuan, and Chia-Chi Huang. "On the architecture and performance of a hybrid image rejection receiver." Selected Areas in Communications, IEEE Journal on 19.6 (2001): 1029-1040.

[3] Ismail, Mohammed, and Olsson, Håkan. "A wide-band RF front-end for multiband multistandard high-linearity low-IF wireless receivers." Solid-State Circuits, IEEE Journal of 37.9 (2002): 1162-1168.

[4] Nassar, Ibrahim T., and Weller, Thomas M. "An electrically small meandered line antenna with truncated ground plane." Radio and Wireless Symposium (RWS), 2011 IEEE. IEEE, 2011.

[5] Katehi, P., and N. Alexopoulos. "On the effect of substrate thickness and permittivity on printed circuit dipole properties." Antennas and Propagation, IEEE Transactions on 31.1 (1983): 34-39.

[6] James, J. R., A. J. Schuler, and R. F. Binham. "Reduction of antenna dimensions by dielectric loading." Electronics Letters 10.13 (1974): 263-265.

[7] Pozar, David M. “Microwave Engineering.” New York: Wiley, 1997. Print.

[8] Bahl, I., Prakash Bhartia, and S. Stuchly. "Design of microstrip antennas covered with a dielectric layer." Antennas and Propagation, IEEE Transactions on 30.2 (1982): 314-318.

[9] Lee, Ming, et al. "Distributed lumped loads and lossy transmission line model for wideband spiral antenna miniaturization and characterization." Antennas and Propagation, IEEE Transactions on 55.10 (2007): 2671-2678.

[10] Wheeler, Harold A. "Fundamental limitations of small antennas." Proceedings of the IRE 35.12 (1947): 1479-1484.

[11] Chu, Lan Jen. "Physical Limitations of Omni-Directional Antennas." Journal of applied physics 19.12 (1948): 1163-1175.

[12] McLean, James S. "A re-examination of the fundamental limits on the radiation Q of electrically small antennas." Antennas and Propagation, IEEE Transactions on 44.5 (1996): 672.

[13] Yaghjian, Arthur D., and Best, Steven R. "Impedance, bandwidth, and Q of antennas." Antennas and Propagation, IEEE Transactions on 53.4 (2005): 1298-1324.

[14] Serway, Raymond, and Jewett Jr., John. “Physics for Scientists & Engineers.” 7th ed. Belmont, CA: David Harris, 2008. Print.

[15] Pucel, Robert A., Daniel J. Masse, and Curtis P. Hartwig. "Losses in microstrip." Microwave Theory and Techniques, IEEE Transactions on 16.6 (1968): 342-350.

[16] Pucel, Robert A. "Design considerations for monolithic microwave circuits." Microwave Theory and Techniques, IEEE Transactions on 29.6 (1981): 513-534.

[17] Ansys, . "HFSS Two-Way Mechanical Coupling for Full-Wave Electromagnetics to Thermal Stress Simulation." Web. 18 Oct 2013. <http://www.ansys.com/staticassets/ANSYS/staticassets/resourcelibrary/presentation/hfss-2way-thermal-dimensions.pdf>.

[18] Parnes, Michael. "The Correlation between Thermal Resistance and Characteristic Impedance of Microwave Transmission Lines." MICROWAVE JOURNAL-EUROGLOBAL EDITION- 43.3 (2000): 82-95.

[19] Bahl, Inder J. "Average power handling capability of multilayer microstrip lines." International Journal of RF and Microwave Computer-Aided Engineering 11.6 (2001): 385-395.

[20] Nassar, Ibrahim T., and Thomas M. Weller. "An electrically-small, 3-D cube antenna fabricated with additive manufacturing." Power Amplifiers for Wireless and Radio Applications (PAWR), 2013 IEEE Topical Conference on. IEEE, 2013.

[21] Gupta, Saurabh, and Gokhan Mumcu. "Dual-Band Miniature Coupled Double Loop GPS Antenna Loaded with Lumped Capacitors and Inductive Pins." Antennas and Propagation, IEEE Transactions on 61.6 (2013): 2904-2910.

[22] Kramer, B. A., C-C. Chen, and J. L. Volakis. "Size reduction of a low-profile spiral antenna using inductive and dielectric loading." Antennas and Wireless Propagation Letters, IEEE 7 (2008): 22-25.

[23] Wang, Johnson JH. "The spiral as a traveling wave structure for broadband antenna applications." Electromagnetics 20.4 (2000): 323-342.

[24] Apaydin, Nil, et al. "Experimental Validation of Frozen Modes Guided on Printed Coupled Transmission Lines." Microwave Theory and Techniques, IEEE Transactions on 60.6 (2012): 1513-1519.

[25] Mumcu, Gokhan, et al. "Small wideband double-loop antennas using lumped inductors and coupling capacitors." Antennas and Wireless Propagation Letters, IEEE 10 (2011): 107-110.

[26] Guraliuc, Anda R., et al. "Numerical analysis of a wideband thick archimedean spiral antenna." Antennas and Wireless Propagation Letters, IEEE 11 (2012): 168-171.

[27] Wheeler, M. "On the radiation from several regions in spiral antennas." Antennas and Propagation, IRE Transactions on 9.1 (1961): 100-102.

[28] Volakis, John L, Chi-Chih Chen, and K Fujimoto. "Small Antennas: Miniaturization Techniques & Applications." New York: McGraw-Hill, 2010. Print.

[29] Nakano, Hisamatsu, et al. "Equiangular spiral antenna backed by a shallow cavity with absorbing strips." Antennas and Propagation, IEEE Transactions on 56.8 (2008): 2742-2747.

[30] Nakano, Hisamatsu, et al. "Low-profile equiangular spiral antenna backed by an EBG reflector." Antennas and Propagation, IEEE Transactions on 57.5 (2009): 1309-1318.

[31] "Stratasys Production Series." Web. 1 Nov 2013. <http://www.stratasys.com/3dprinters/production-series>.

[32] O'Brien, Jonathan. Rojas, Eduardo. Weller, Thomas. "A switched-line phase shifter fabricated with additive manufacturing." International Microelectronics Assembly and Packaging Society. (2013)

Appendices

Appendix A Tapered Balun Design and Measured Results

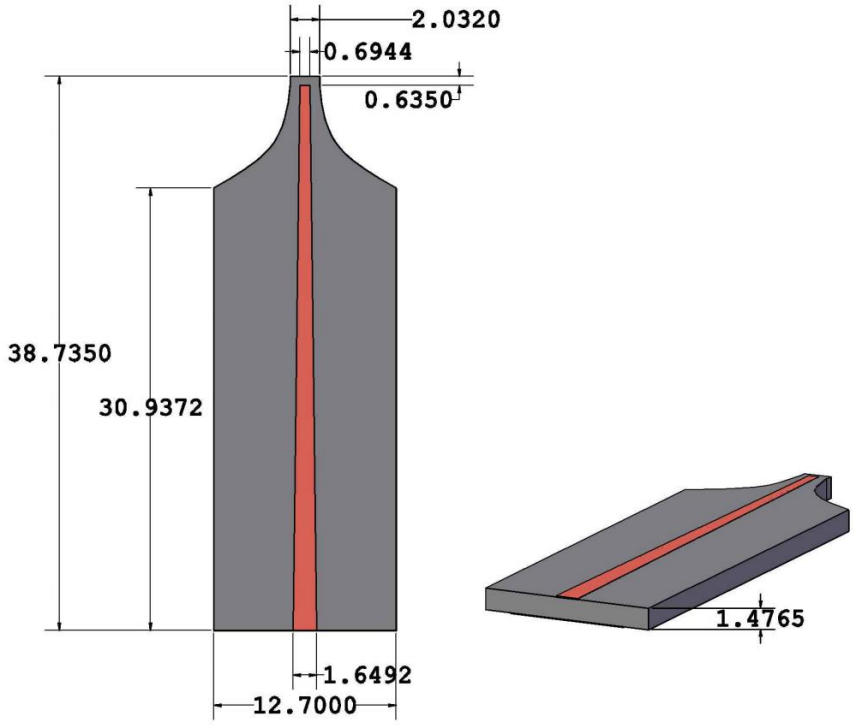

Figure A.1: Top and profile view of balun showing dimensions in mm

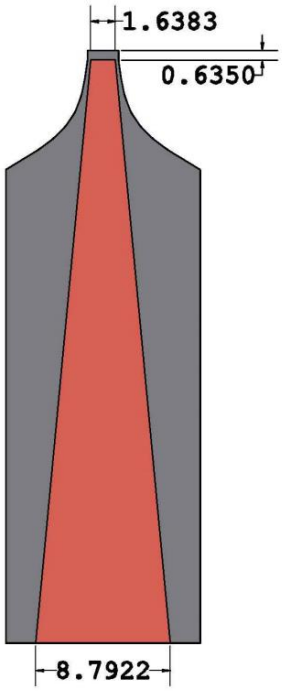

Figure A.2: Bottom view of balun showing dimensions in mm

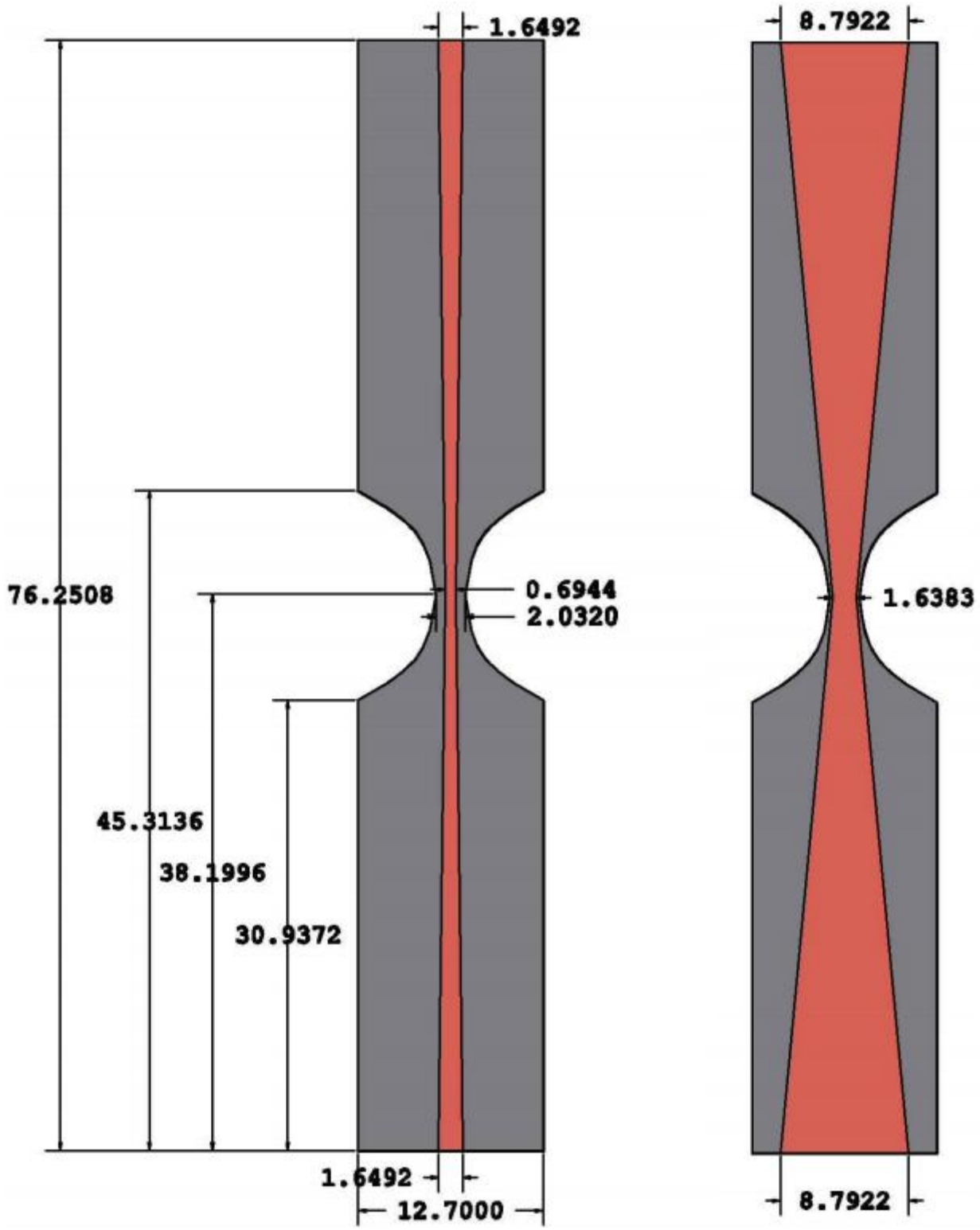

Figure A.3: Top and bottom view of back to back balun used for measurement and simulation verification showing dimensions in mm

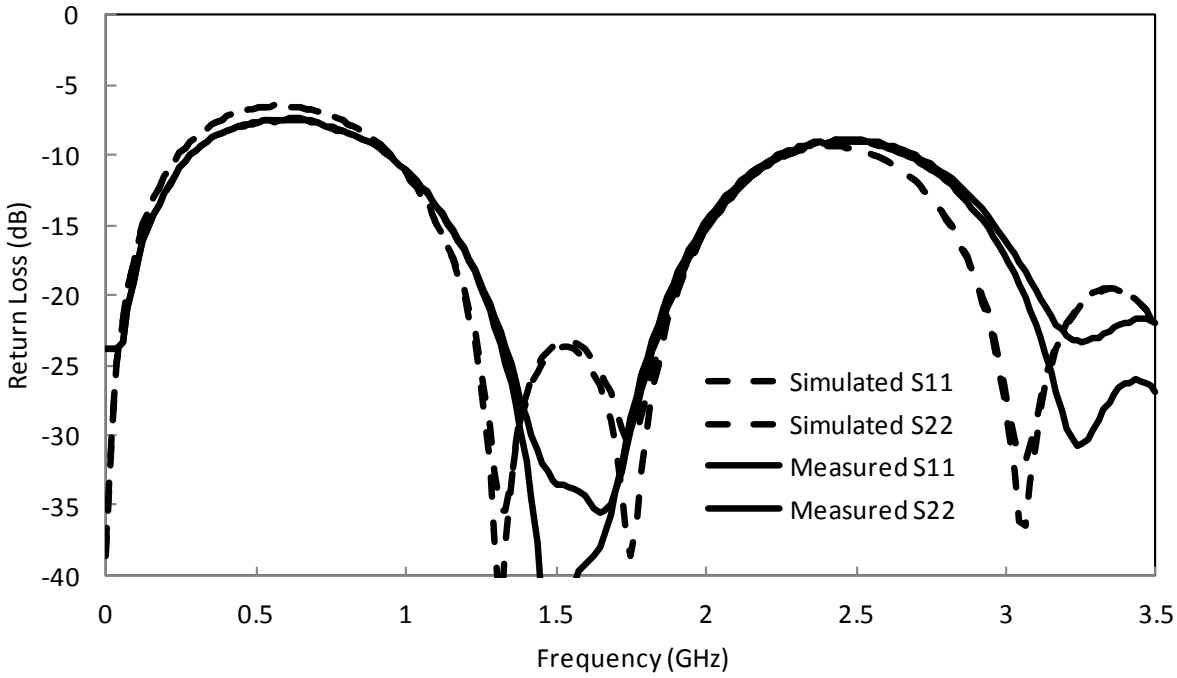

Figure A.4: Measured and simulated return loss of back-to-back balun used for performance verification

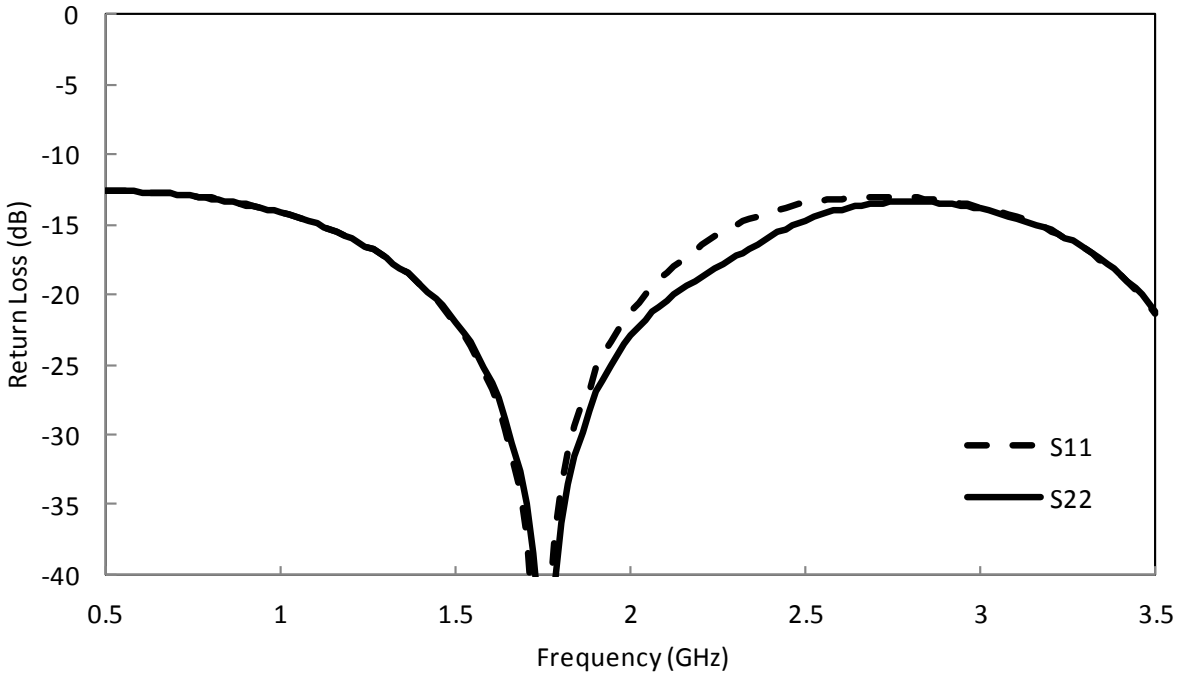

Figure A.5: Simulated return loss of single balun used to feed both PSA antenna models

About the Author

Jonathan O'Brien received his B.S. degree in Electrical Engineering in 2012 from the University of South Florida. Towards the end of his bachelor's degree, he worked for a small engineering company tasked with designing self-test systems for the Orion Shuttle project. His graduate studies were first sponsored by nScrypt and Sciperio. During this time, he researched and characterized additive manufactured materials for RF applications. He was then the recipient of a Draper Labs fellowship where he concentrated on advanced antenna design.